Title: Microbial communities increase host plant leaf growth in a pitcher plant experimental system

Authors: Jessica R. Bernardin[1], Erica B. Young[2], Sarah M. Gray[3], Leonora S. Bittleston[1]

Addresses: [1]Department of Biological Sciences, Boise State University, Boise, Idaho, USA, [2]Department of Biological Sciences and School of Freshwater Sciences, University of Wisconsin-Milwaukee, Milwaukee, Wisconsin, US, [3]University of Fribourg, Department of Biology-Ecology and Evolution, Fribourg, Switzerland

Corresponding author contact information: jessicabernardin@boisestate.edu

Abstract

Across diverse ecosystems, bacteria and their host organisms engage in complex relationships having negative, neutral, or positive interactions. However, the specific effects of leaf-associated bacterial community functions on plant growth are poorly understood. To address this gap, we explored the relationships between bacterial community function and host plant growth in the purple pitcher plant (*Sarracenia purpurea*). The main aim of our research was to investigate how different bacterial community functions affect the growth and nutrient content in the plant. Previous research had suggested that microbial communities may aid in prey decomposition and subsequent nutrient acquisition in carnivorous plants, including *S. purpurea*. However, the specific functional roles of these bacterial communities in plant growth and nutrient uptake are not well known. In this study, sterile, freshly opened leaves (pitchers) were inoculated with three functionally distinct, pre-assembled bacterial communities and effects examined over 8 weeks. Bacterial community composition and function were measured using physiological assays, metagenomics, and metatranscriptomics. Distinct bacterial functions affected plant traits; a bacterial community enriched in decomposition and secondary metabolite production traits was associated with larger leaves with almost double the biomass of control pitchers. Physiological differences in bacterial communities were supported by metatranscriptomic analysis; for example, the bacterial community with the highest chitinase activity had greater expression of transcripts associated with chitinase enzymes. The relationship between bacterial community function and plant growth observed here indicates potential mechanisms for host-associated bacterial functions to support plant health and growth.

Importance

This study addresses a gap in understanding the relationships between bacterial community function and plant growth. We inoculated sterile, freshly opened pitcher plant leaves with three functionally distinct bacterial communities to uncover potential mechanisms through which bacterial functions support plant health and growth. Our findings demonstrate that distinct bacterial functions significantly influence plant traits, with some bacterial communities supporting more growth than in control pitchers. These results highlight the ecological roles of microbial communities in plants and thus ecosystems, and suggest potential pathways in which microbes support host plant health. This research provides valuable insights into plant-microbe interactions and effects of diverse microbial community functions.

Keywords

microbial community function; metatranscriptomics; phyllosphere; microbe-plant interactions; host health; metagenomics; pitcher plant; *Sarracenia purpurea*

Introduction

Microbiomes have strong effects on the health and fitness of their hosts (1, 2). Host plant growth and physiology are influenced by the presence of leaf-associated (phyllosphere) microbes, with microbial taxa acting as mutualists, commensals, and antagonistic pathogens (3–6). Phyllosphere microbes live in complex microecosystems (7, 8) performing functions that contribute to plant nutrient acquisition, phytohormone production, and stress tolerance (3).

For example, the addition of synthetic phyllosphere communities was shown to increase fruit production in greenhouse-grown tomatoes (6) and increase leaf sugar content and metabolic diversity in field-grown *Agave tequilana* (9). Plants reap many benefits from hosting microbial communities (3, 9). Nutrient cycling interactions between microbes and plants can occur directly, e.g., via bacterial nitrogen fixation, and indirectly, e.g., via increased bacterial growth that influences host plant metabolism (3, 10). Many bacteria associated with plant-microbe interactions also have pathways to produce phytohormones, like auxin or cytokinins, which support plant cell metabolism and growth (3, 11–15). Plant growth-promoting bacteria can also mediate host stress responses, including increasing drought tolerance, thermotolerance, and UV protection (3, 16, 17). Despite these demonstrated benefits to host plants, we still lack research directly connecting bacterial community function with host physiological functions and benefits. We define bacterial community function as the collective metabolic processes of all the individual bacteria within a community. We addressed this knowledge gap by examining both bacterial and plant physiology, using metabarcoding, metagenomics, and metatranscriptomics of bacterial communities and measuring plant responses.

The carnivorous pitcher plant, *Sarracenia purpurea* L., uses water-filled, cup-shaped leaves to trap and digest insects to supplement acquisition of nutrients from low nutrient soils (18, 19). These leaves or 'pitchers' host an aquatic micro-ecosystem composed of microbes, fungi, protists, and invertebrates (8, 20, 21). The microbes are thought to provide critical ecosystem functions to the host plants by mediating insect prey digestion through the production of extracellular hydrolytic enzymes. It is likely that the bacterial production of protease and chitinase enzymes that digest protein and chitin-rich insect prey are especially important for this carnivorous plant species (22–24). *Sarracenia purpurea* pitcher plants do not produce chitinase enzymes (22). Thus, they may rely heavily on the bacterial extracellular enzymes to catalyze decomposition of insect prey and support the mineralization of carbon, nitrogen, and other nutrients for the host plant and the whole micro-ecosystem. This is an ideal model system to examine bacterial functions in controlled manipulative experiments, serving as an analog for other systems where experimentation is more challenging. Although previous research has hypothesized that pitcher plant leaf-associated bacterial communities benefit the host plant (18, 25, 26), no studies have specifically measured a direct benefit to the plant.

To connect the effects of bacterial function to plant growth, we designed a manipulative experiment using pitcher plant leaves and bacterial communities with different physiological functional profiles, measured as different levels of activity across different physiological functions (Fig. S1). These community physiological functions, including hydrolytic enzyme activity, organic substrate use, and respiration rates, were characterized for the three distinct experimental bacterial communities prior to inoculation, and the effects of these functionally distinct bacterial communities on host plants, were examined over eight weeks (Fig. 1).

We asked four specific questions:

1) Do bacterial communities with different functional profiles have differential effects on plant traits, such as leaf growth and nutrients?

2) Are there taxonomic characteristics of these bacterial communities that can explain the observed functional differences?
3) Can bacterial functions directly measured with physiological assays be linked with differential gene expression (metatranscriptomics) to better understand how bacterial community function impacts their host?
4) Are there specific functions, e.g., hydrolytic enzyme activity or carbon substrate use, that drive these effects on host plants?

We hypothesized that communities with specific physiological functions (e.g., high chitinase activity) would differentially express genes related to degradation, helping to release and make available more nutrients to enhance host plant growth.

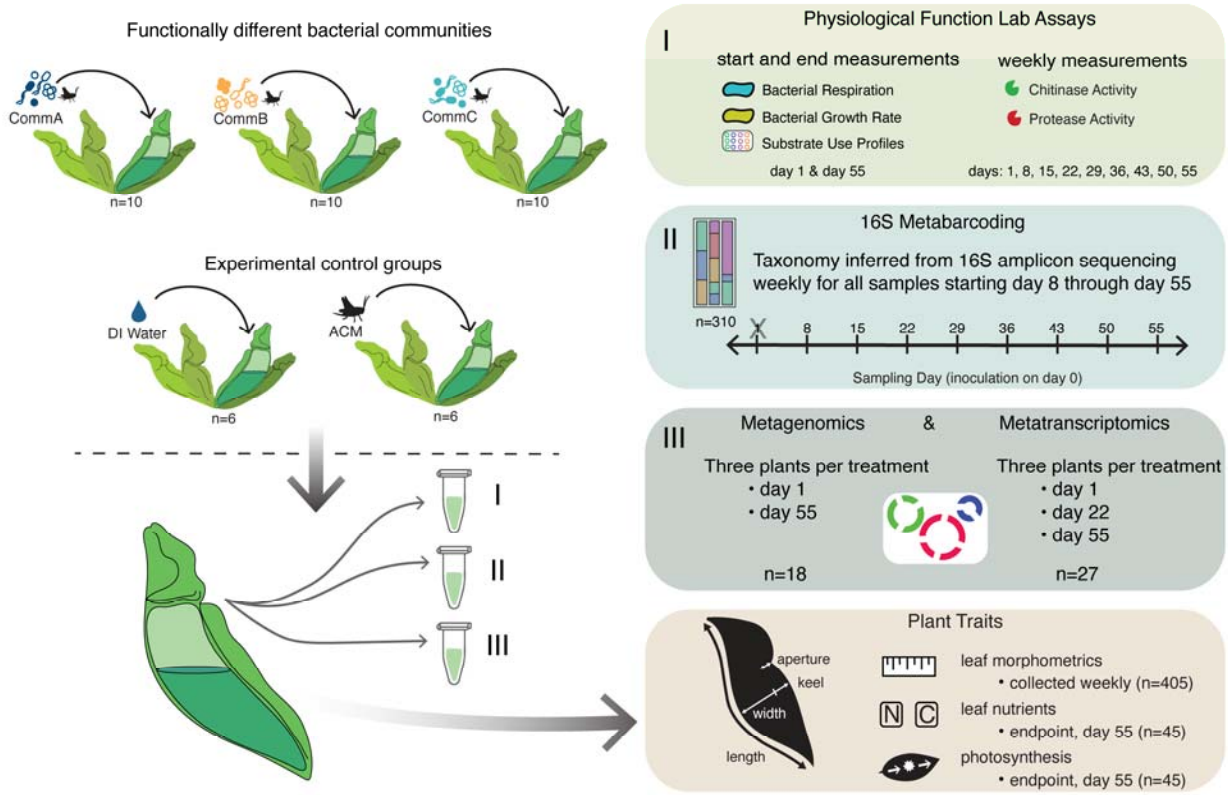

Figure 1. Experimental design. Three functionally distinct bacterial communities (CommA, CommB, and CommC) growing in sterile acidified cricket media (ACM) were inoculated into sterile pitchers and plants incubated in growth chambers for eight weeks. Sterile deionized (DI) water or ACM were added to additional pitchers as experimental controls. Pitcher fluid samples were collected weekly to characterize bacterial community composition and function: chitinase and protease activity, community respiration, growth rate, organic substrate use profiles, 16S amplicon sequencing, metagenomics, and metatranscriptomics. Plant functional traits were also assessed, including morphometric measurements of pitchers, as well as end-of-experiment measures of leaf biomass, leaf nutrient content, and photosynthetic rate.

Results

125 **Starting communities were functionally different**
126 The three communities (CommA, CommB, and CommC) inoculated into pitchers were
127 functionally different in their chitinase activity, protease activity, bacterial respiration, and/or
128 EcoPlate organic carbon substrate use profiles (Fig. 2, Fig. S2). Prior to inoculation, CommB had
129 the highest chitinase activity and lowest protease activity (Fig. 2A, B, statistical differences
130 shown in Fig. S2), and bacterial respiration was lower in CommB than the other two
131 communities (Fig. S2). Using a permutational multivariate analysis of variance (PERMANOVA),
132 we observed strong differences in carbon substrate use profiles among the three bacterial
133 communities, both in the community cultures prior to inoculation (day 0) and when resampled
134 from the pitchers 24 hours after inoculation (day 1) (Fig. 2C, Fig. S3, Table S1). CommB was the
135 most distinct, while CommA and CommC exhibited similar levels of hydrolytic enzyme activity,
136 all three communities had distinct carbon substrate use profiles. We found significant
137 differences in community composition between the treatments on day 1 based on
138 metagenomic sequencing (Fig. 2D, PERMANOVA; R^2=0.78, $F_{2,8}$=10.382, P=0.005). There were no
139 measured differences in bacterial community growth rates prior to inoculation or at any point
140 during the experiment (Fig. S2).
141

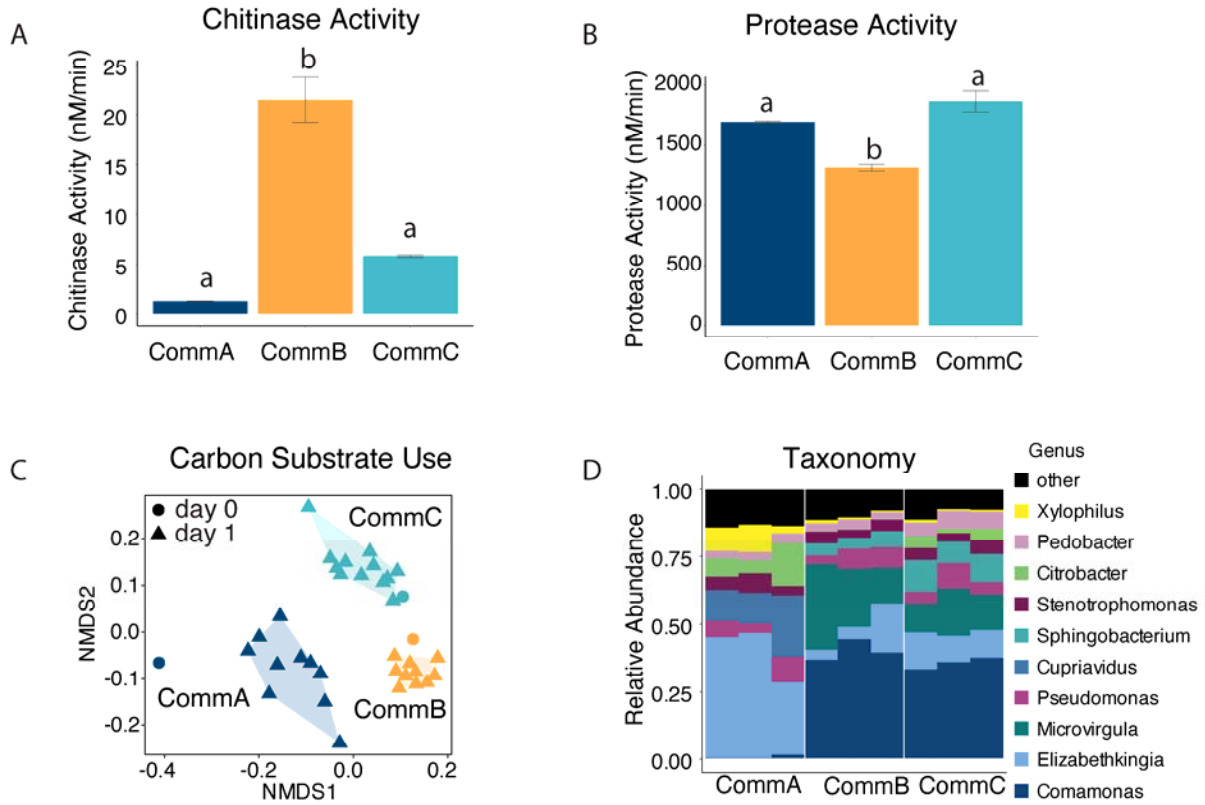

142
143 Figure 2. The three bacterial communities had different physiological functions measured
144 before pitcher inoculation. (**A**) CommB had higher chitinase activity and (**B**) lower protease
145 activity than CommA and CommC, there were no differences in bacterial growth rates between
146 the starting treatments and CommB had the lowest bacterial respiration rates (Fig. S2). (**C**) The
147 three communities also showed different EcoPlate carbon substrate use profiles, using Bray-
148 Curtis dissimilarity and visualized with a NMDS (k=2, stress=0.138) at day 0 prior to inoculation

149 and on day 1, 24 hours after inoculation. (**D**) These three communities also had distinct
150 bacterial compositions (top 10 genera shown) at day one, based on taxonomy from shotgun
151 metagenomic sequencing.
152
153 **Bacterial function affects plant traits**
154 To investigate the influence of functionally diverse bacterial communities on plant traits
155 (Question 1), we evaluated how experimental treatments (CommA, CommB, and CommC) and
156 control treatments (water and ACM) affected pitcher biomass and nitrogen content after the
157 plants hosted the treatments for an 8-week period. We compared our treatment communities
158 to two control groups to help parse out differences between the effect of hosting the bacterial
159 community vs. the media they are grown in, since pitcher plants may be able to directly absorb
160 amino acids from degraded prey items (27). Pitchers hosting CommB had 1.7 times higher
161 biomass (mean biomass = 0.47 g) than pitchers with cricket media only (mean biomass = 0.28 g)
162 and 2 times higher biomass than the water-only plants (mean biomass = 0.23 g, Fig. 3A, 3B). We
163 observed that plants that hosted CommB had higher biomass (Fig. 3A, 3B), longer pitcher
164 length, and higher carbon content (Fig. S4) than not only the water and media controls, but also
165 the other experimental treatments, CommA and CommC. While pitchers size varied and the
166 sample size was relatively low due to the slow growth of this perennial plant (n=46), the
167 probability of observing a higher pitcher biomass in bacterial community treatments compared
168 to the cricket media (ACM) control was estimated at 81.0% for CommA, 99.7% for CommB, and
169 84.3% for CommC (based on posterior probabilities from GLMM, Fig. 3B). Although the 95%
170 credible intervals (CIs) contained zero for CommC, we also saw a trend of a positive effect on
171 total plant growth (measured as the net production of leaves). Plants in the CommC group had
172 an estimated 1.4 greater net (gross new leaves - gross leaf loss) new pitcher production
173 compared to the ACM control over eight weeks (Fig. S4).
174
175 Bacterial communities and the ACM control also affected nitrogen levels in pitcher plants (Fig.
176 3C and 3D). Comparing total pitcher nitrogen content between the treatment groups and the
177 two controls (ACM, water), there was a 74% probability that bacterial treatments had higher
178 nitrogen content than the ACM treatment, although the 95% credible intervals included zero.
179 Water had a strong negative effect on pitcher nitrogen content, with plants containing only
180 water having an estimated 1.7 mg of nitrogen, those with ACM having 4.2 mg, and those in the
181 three bacterial treatments averaging 5.2 mg (Fig. 3C and 3D). We found no impact of the
182 bacterial community treatment groups on other plant traits, including photosynthetic rates and
183 photosynthetic quantum yield (F_v/F_m) (Fig. S4).
184

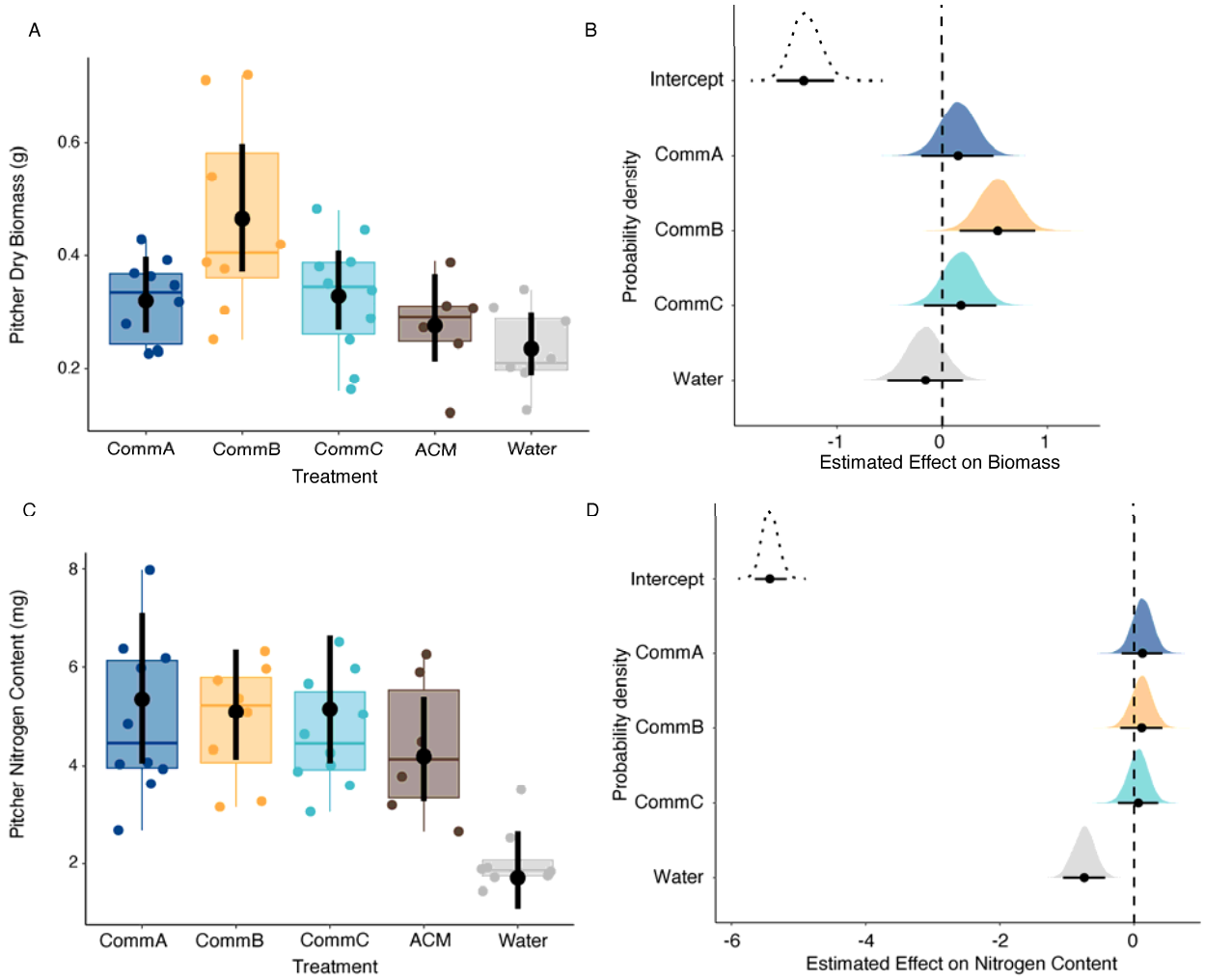

Figure 3. Bacterial community treatment affects plant traits. (**A**) Bayesian GLMM marginal effects of treatment on target pitcher biomass are represented by the black points, which are the median estimates, and the vertical lines represent the 95% credible intervals (CIs). The pitcher biomass data used to calculate estimated effects are represented by the box plot and colored points behind the marginal effect estimates. (**B**) Predicted effects of functionally distinct community treatments on pitcher biomass. Black points represent median estimates, lines represent the 95% CIs, and color-coded (by treatment) density plots indicate the full posterior. The intercept (dashed posterior) is set as the ACM baseline. (**C**) Bayesian GLMM marginal effects of treatment on pitcher nitrogen content, and (**D**) predicted effects of bacterial community treatments on pitcher nitrogen content.

Compositional differences between the three communities — 16S metabarcoding results

After quality control and rarefaction, we recovered 917 amplicon sequence variants (ASVs) in a community matrix spanning 310 samples (6-10 pitchers per treatment across 8 weekly time points). These ASVs represented 26 bacterial phyla, 192 families, and 286 genera. Among the 20 most abundant genera averaged across pitchers within a treatment at a single time point,

202 *Microvirgula* (14.2%), *Stenotrophomonas* (12.4%), and *Pedobacter* (11.3%) accounted for
203 almost 25% of reads (Fig. 4A).
204
205 **Community Diversity and Differential Abundance**
206 Addressing Question 2 with regard to taxonomic characteristics of the bacterial communities
207 that could explain functional differences, we first observed differences in alpha diversity
208 between the three treatments after one week *in planta* (Fig. 4B, Fig. S5). Between days 8 and
209 55, the effective number of ASVs increased (with a mean gain of 7.5 ASVs per sample) and by
210 day 55, the differences in ASV numbers between community treatments had disappeared (Fig.
211 4B, Fig. S5). Beta diversity was different between the three community treatments
212 (PERMANOVA; R^2=0.282, $F_{2, 214}$=42.04, p=0.001) using unweighted UniFrac distances, shown as
213 clear clustering of treatments in NMDS visualization (Fig. 4C) and significant pairwise
214 differences over time (Table S2). Mantel tests (Spearman's rank correlation rho) showed
215 significant correlations between the unweighted UniFrac distances of 16S community diversity
216 with chitinase activity (r=0.227, p=0.001) and with final pitcher length (r=0.117, p=0.001), but
217 no significant relationship with protease activity (r=0.004, p=0.44) or pitcher dry biomass
218 (r=0.166, p=0.066).
219
220 Analysis of compositions of microbiomes with bias correction (ANCOM-BC) (28) identified 38
221 differentially abundant taxa between treatments (Table S3) with log fold changes (LFC) greater
222 than 1.5 between at least one pair of treatments (CommB vs. CommA, CommC vs. CommA, or
223 CommB vs. CommC). These taxa were plotted along with error estimates (Fig. 4D). In our
224 model, CommB is set as the reference, so negative log fold change values indicate increased
225 abundance in CommB (Fig. 4D, left side). CommB had a higher abundance of 13 taxa, with 12 of
226 these taxa showing higher abundance in CommB compared to CommA, and 1 taxon showing
227 higher abundance in CommB compared to CommC. Conversely, CommB had significantly lower
228 abundance in 6 other taxa (Fig. 4D).

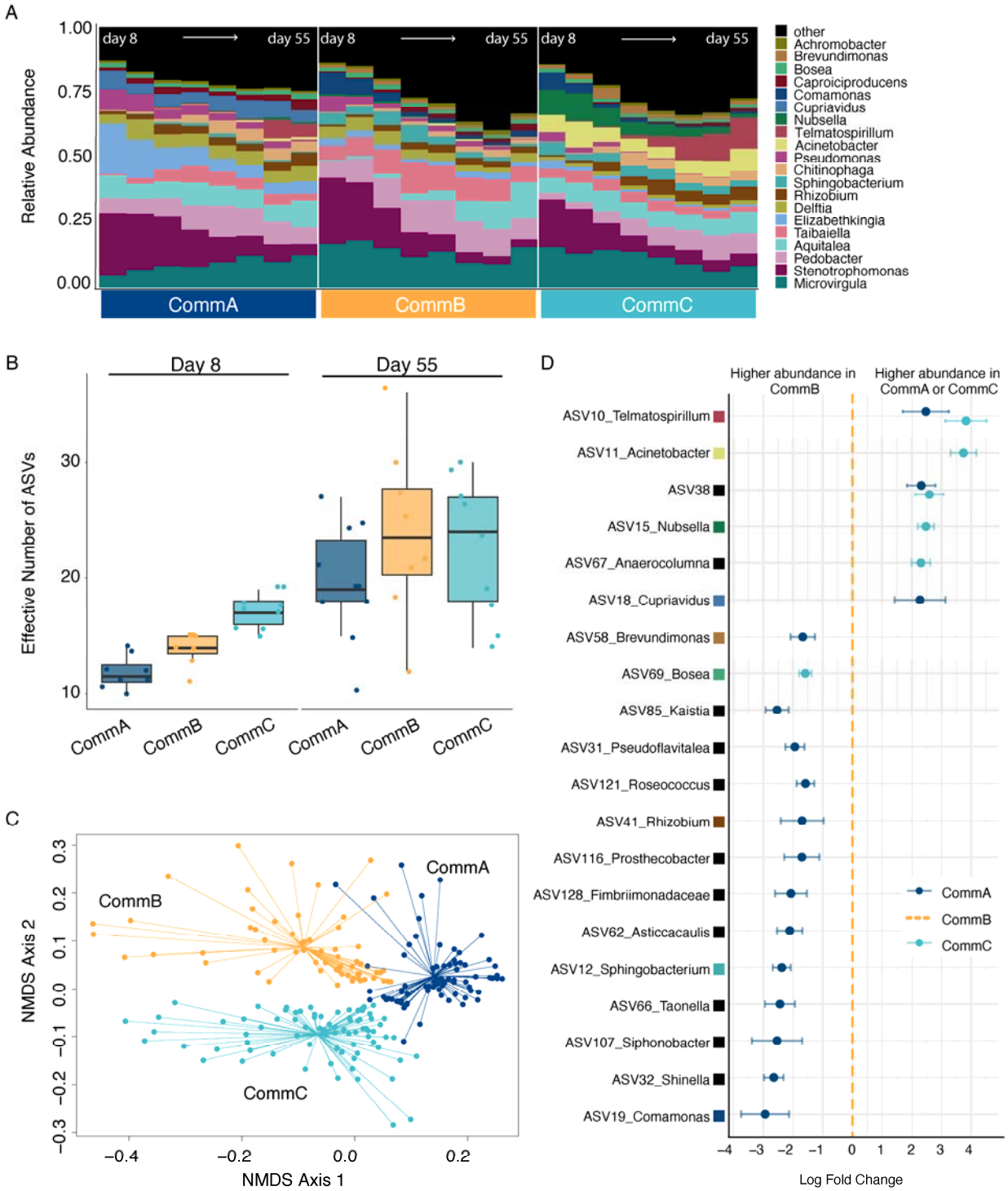

Figure 4. Bacterial community compositional differences between the three bacterial community treatments, based on 16S amplicon sequencing. (**A**) Relative abundance of the 20 most abundant genera from day 8 to 55 (days: 8, 15, 22, 29, 36, 43, 50, 55), with reads averaged for 10 different pitchers at the same time point. (**B**) Effective number of ASVs (Hill number 1) for each treatment at day 8 and day 55; box plots show the interquartile range, the horizontal lines are the median values and the whiskers extend 1.5 times the interquartile

range, and each point represents a pitcher fluid sample. (**C**) Composition-based NMDS calculated using unweighted UniFrac for all samples within each of the three treatments from day 8 to 55, stress=0.17, k=2. (**D**) Twenty differentially abundant ASVs, predicted from ANCOM-BC2 (subset of ASVs with a log fold change greater than +/- 1.5) with CommB as the reference (orange dashed line). Points are colored by treatment and represent the log fold change of the model effects, with whiskers representing the standard error around each estimate. ASVs are labeled with assigned genus when available, and each colored square matches the color key in (**A**).

Linking bacterial physiology with agnostic estimates of functional expression

To address Question 3, we identified 218,817 transcripts from 27 metatranscriptomic samples, including 3 pitchers each for 3 bacterial treatments at 3 different time points (Figure 1). This analysis links bacterial functions directly with differential gene expression (metatranscriptomics). After filtering out transcripts lacking KEGG orthologs, 162,624 total transcripts remained. We visualized the differences in metatranscriptomic profiles between the three bacterial treatments over time using an NMDS based on Bray-Curtis dissimilarities for all transcripts (Fig. 5A). We found clear differences between treatments (PERMANOVA; R^2=0.20 $F_{2, 22}$=4.46, p=0.001), despite the many shared transcripts, and clear patterns through time (PERMANOVA; R^2=0.27, $F_{2, 22}$=6.00, p=0.001). The transcript by sample matrix of ~162,000 genes was normalized and put into our differential expression (DE) model, which identified 24,357 unique significantly differentially expressed genes between our three bacterial communities.

Each treatment had unique and shared transcripts (Fig. 5B). Comparison of differential expression between treatments using pairwise contrasts showed 5,767 transcripts with positive log fold change for CommA, and 10,885 with negative log fold change for CommA relative to the mean of CommB and CommC. For CommB, 2,124 transcripts had positive log fold change, and 4,278 had negative log fold change. CommC had 5,851 transcripts with positive log fold change, and 6,257 had negative log fold change, relative to the mean of CommA and CommB. To get an agnostic view of functional expression between treatments, we plotted the model estimate of mean average expression and log fold change for each transcript in each treatment contrast, and color coded according to p-value (Fig. 5D, 5E, 5F). We averaged the log fold change for transcripts mapping to the same KEGG function and ranked them from high to low in order to find the most differentially expressed functions in each treatment (Fig. 5G, 5H, 5I).

In CommA, we found high expression of functions related to phenol/toluene 2-monooxygenase, aminomuconate-semi aldehyde, and 2-oxo-3-hexenedioate decarboxylase, related to aromatic compound degradation (Fig. 5G). For CommB, we found high expression of functions for xylobiose transport system substrate-binding protein, basic endochitinase B, and fructose-6-phosphate phosphoketolase (Fig. 5H). We found support for our physiological measures of high chitinase activity (Figs. 1A and 6A), with basic endochitinase B being one of the top 5 highly expressed functions for CommB. For CommC, there was high expression of functions related to proton-translocating transhydrogenase, glycerol-3-phosphate O-acyl transferase, and very long chain acyl-CoA dehydrogenase, related to fatty acid metabolism (Fig. 5I).

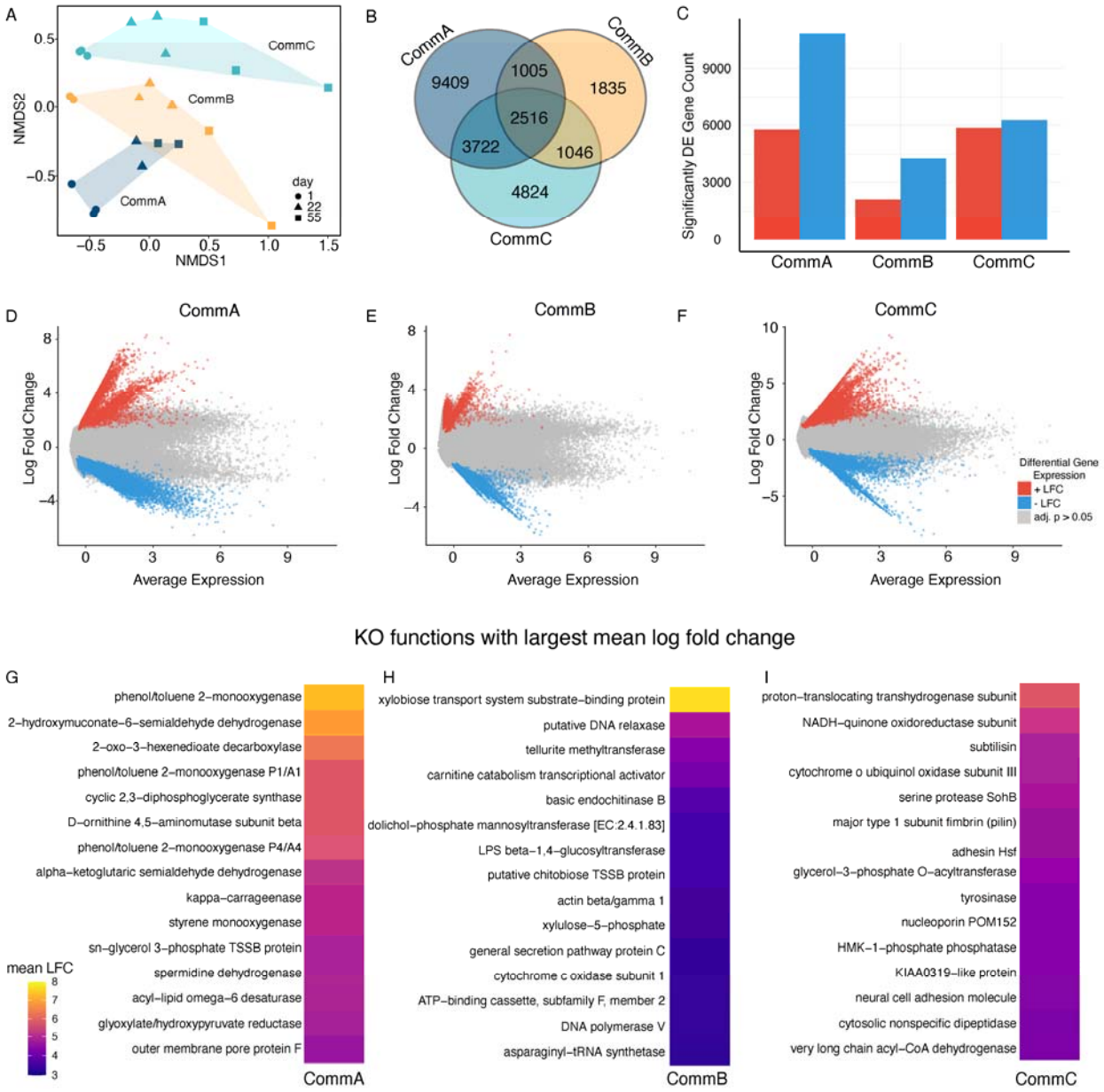

Figure 5. Treatment communities had distinct patterns of gene expression. (**A**) Transcript-based NMDS calculated using Bray-Curtis dissimilarities for all samples within each of the three treatments at days 1, 22, and 55, stress=0.099, k=2 (PERMANOVA, R^2=0.0.20, $F_{2,22}$=4.46, p = 0.001). (**B**) Venn diagram showing the shared and unique differentially abundant transcripts among the three bacterial communities. (**C**) Bar plot displaying the count of differentially expressed (DE) genes (up regulated in red and down-regulated in blue) between the three bacteria community treatments, highlighting significant differences in gene expression between each community based on community contrasts in our differential expression model. (**D, E, F**) The mean abundance (MA) plots depict the log fold change (LFC) versus the predicted average expression of transcripts for each treatment based on our differential expression model, (**D**) CommA, (**E**) CommB, (**F**) and CommC, (red points are positive LFC, blue are negative LFC, gray

293 are adjusted p-value > 0.05). (**G, H, I**) Heat maps illustrating the 20 most abundant KEGG KO
294 functions, based on the differentially expressed genes averaged within each KEGG Orthology
295 (KO) function for each treatment, (**G**) CommA, (**H**) CommB, and (**I**) CommC. The KOs were
296 ranked from high to low mean log fold change.
297
298 **Linking bacterial physiology with hydrolytic enzyme functional expression**
299 Beyond the general functional differences identified by differential transcription, specific
300 functions related to hydrolysis were examined. We measured chitinase as chitobiosidase and
301 protease as L-amino-peptidase enzyme activities, analyzing only the 9 pitchers which also had
302 metatranscriptomics (3 of 10 plants per treatment). Over 8 weeks, CommA had lower chitinase
303 activity, compared to CommB and CommC (Fig. 6A, Fig. S6). This result was similar to
304 physiological assays in the bacterial communities prior to inoculation (Fig. 1A), but in this
305 smaller subset across time, CommB and CommC were not statistically different. Protease
306 activity in the 9 pitchers was consistent with community assays prior to inoculation, with
307 CommB showing lower protease activity than CommA and C (Fig. 6B, Fig. S6).
308
309 We used metatranscriptomic data to explore hydrolysis functions in two ways. First, we
310 investigated the transcript abundances for differentially expressed genes that mapped to
311 chitinase or protease functional KOs. Second, we paired these abundance measures with the
312 log fold change predicted by our differential expression (DE) model. Within this model,
313 contrasts were created to compare the expression levels of each community treatment against
314 the average of the other two (see Fig. 6 legend and methods). This allowed us to identify genes
315 that were differentially expressed in one treatment relative to the others. In Figure 6C, we
316 show all significant DE genes mapping to chitin degradation or transport KOs, including
317 endochitodextinases, endochitinases, exochitinases, and chitin transport systems and putative
318 chitinases. CommB had higher transcript abundances of these chitin related genes, including 12
319 genes with higher expression in CommB, compared to only six chitin-related genes with higher
320 expression in CommA, and only seven in CommC. Similar patterns emerged with normalized
321 transcript abundance for these same genes (log transformed transcripts per million) (Fig. 6C,
322 left side). In Figure 6D, we show many significant DE genes mapping to protein degradation,
323 including general aminopeptidases, leucyl aminopeptidases, tetrahedral aminopeptidases, and
324 tripeptide aminipeptidases. CommB had lower expression of genes related to protease
325 enzymes, two genes with higher expression in CommB, compared to 12 protease related genes
326 with higher expression in CommA, and seven genes for CommC.
327

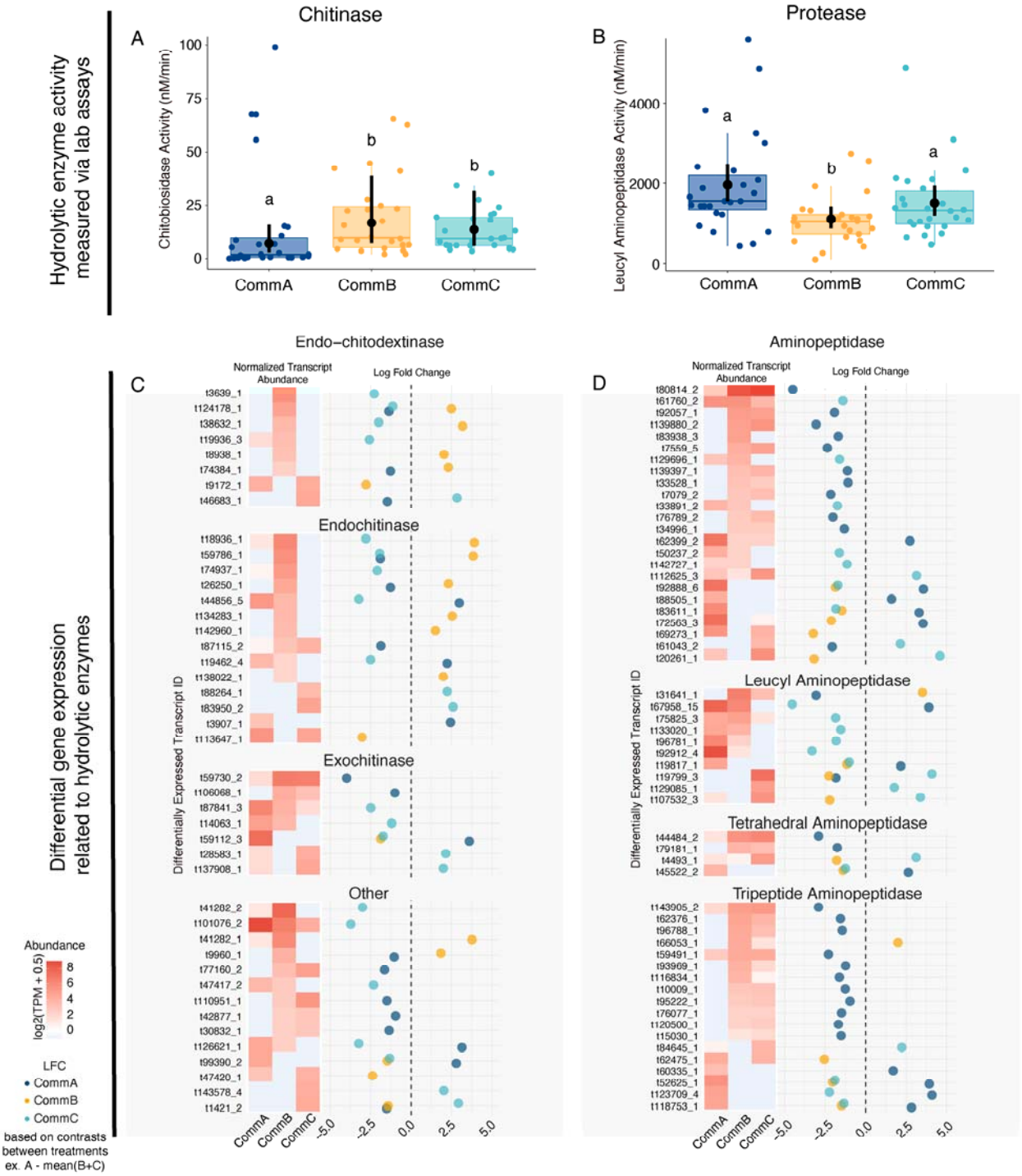

Figure 6. Functional assays of hydrolytic enzyme activity generally matched well with transcript levels of genes related to those functions. (**A, B**) Enzyme activity measured in communities from nine pitcher plants whose samples also underwent downstream metatranscriptomic analysis (within a treatment, three plants x 9 weeks, n=27). Box plots and colored points represent the raw data, with the horizontal bar representing the median values and whiskers

335 showing the 1.5 times the interquartile range. The black points represent the median marginal
336 effects from the model testing the effect of treatment enzyme activity with week as a random
337 intercept, the black vertical bars represent the 95% credibility intervals around each estimate.
338 (**C, D**) Chitinase and protease related transcript comparisons: Within each panel, log fold
339 change (LFC, right) and normalized transcript abundance (TPM, left) of transcripts associated
340 with chitin metabolism KOs (**C**) and protein metabolism KOs (**D**) determined from significantly
341 differential transcript abundances. The log fold change points are colored by treatment and
342 represent the effect size from the differential expression model. The absence of a point for a
343 treatment indicates that the transcript is not differentially expressed for that contrast.
344
345 **Linking bacterial physiology with carbohydrate and amino acid metabolic functions**
346 Carbon substrate use profiles were significantly different among all pairwise combinations of
347 the three treatments on both day one and day 55 (PERMANOVA pairwise differences, $p < 0.05$,
348 Fig. S3, Table S1). Out of the 31 carbon substrates tested, the three communities exhibited
349 differential capacity to use nine (Fig. 7A, Fig. S7). CommB had statistically higher use of N-acetyl
350 glucosamine, beta methyl glucoside, cellobiose, and pyruvic acid methyl ester. CommA showed
351 the highest use of Tween 80, serine, and threonine. Meanwhile, CommC exhibited higher use of
352 galactonic acid gamma lactone and glucosaminic acid.
353
354 Relating carbon substrate use from EcoPlate functional assays, we identified significantly
355 differentially abundant transcripts related to carbohydrate and amino acid metabolism (Fig.
356 7B,C) and aggregated transcript counts by KO function. Because CommB had the largest
357 positive effect on pitcher biomass, we highlighted functions where CommB exhibited markedly
358 higher expression than either CommA or C by at least $\log_2 = 4$ transcripts per million (TPM). We
359 identified 54 KOs that were higher in CommB, many of which are related to the metabolism or
360 transport of carbohydrates like fructose, glucose, and chitin. Additionally, we identified 33 KOs
361 that were higher in CommB, including the enzymes urea carboxylase, nitrile hydratase, and
362 argininosuccinate lyase. These are related to N cycling, contributing to the breakdown and
363 recycling of nitrogen-containing compounds (29, 30).
364

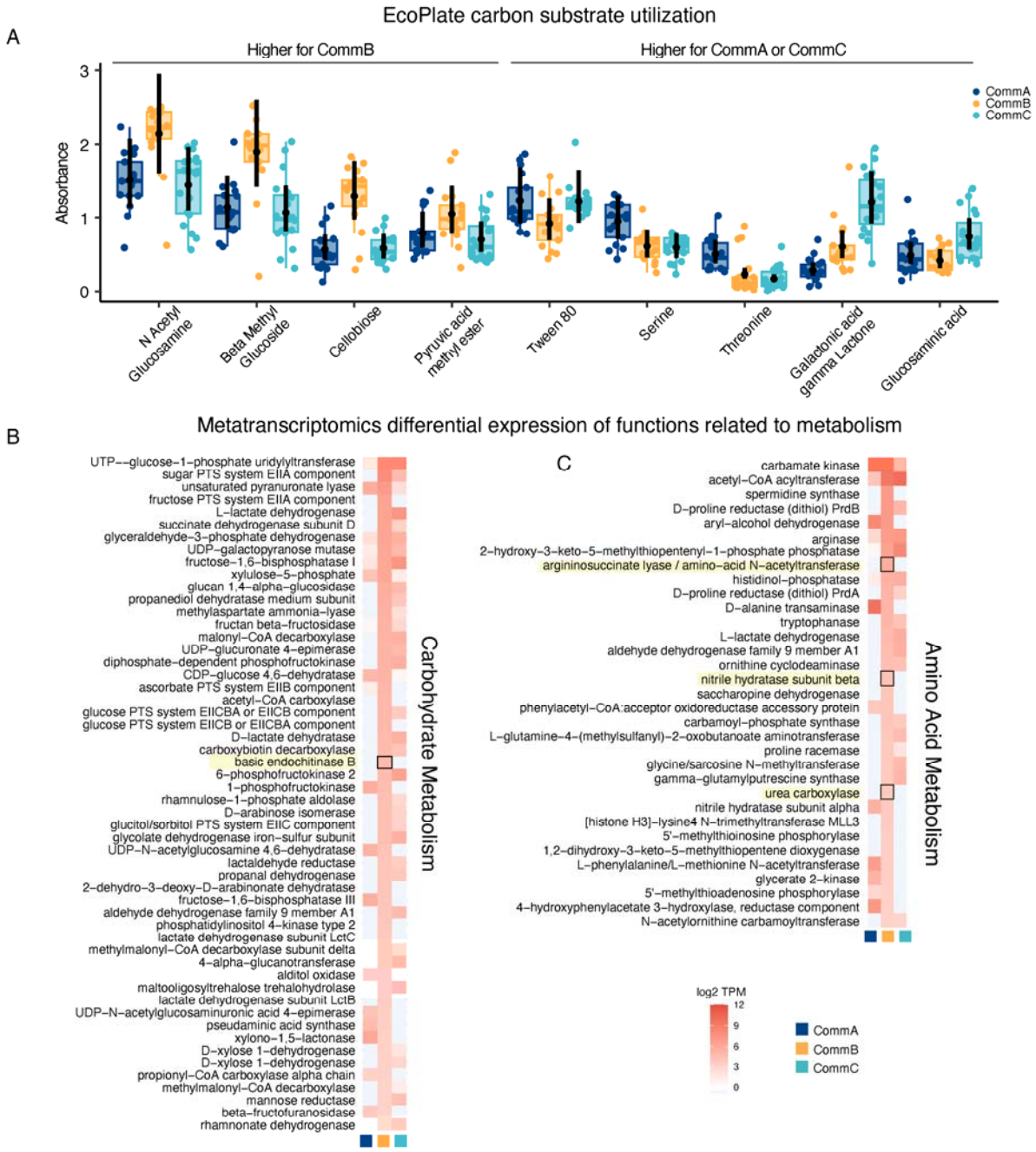

Figure 7. Differences in EcoPlate carbon substrate metabolism among the three treatments. (**A**) A subset of nine of the 31 carbon substrates which showed differences in absorbance among samples of the three treatments. Points are colored by treatment and represent the absorbance for an individual sample for that substrate, day 1 and day 55 samples combined for each substrate. Box plots and colored points represent the raw data, colored whiskers representing data 1.5 times the interquartile range. The black points represent the median marginal effects from the model testing the effect of treatment and substrate on absorbance with week as a random intercept, the black vertical bars represent the 95% credibility intervals around each estimate. (**B, C**) Normalized abundance of KOs associated with (**B**) carbohydrate

375 metabolism and (**C**) amino acid metabolism, using significantly differentially abundant genes
376 summed according to KO function. Heat maps are grouped by treatment and transcripts per
377 million (TPM) are transformed (log2(TPM+0.5)). This subset of KO functions show instances
378 where expression in CommB was significantly higher (by at least 4 log2(TPM+0.5)) than either
379 CommA or CommC. Functions that are particularly relevant for this study are highlighted in
380 yellow.
381
382 **Connecting community functions to metagenome-assembled genomes**
383 In addition to the 16S amplicon sequencing to identify taxa present, we conducted shotgun
384 metagenomic sequencing of 18 samples (3 plants per treatment at day 1 and day 55). The
385 resulting data were used to quantify taxonomy and build high-quality metagenome-assembled
386 genomes (MAGs), which were then connected to the metatranscriptomics data, focusing
387 on hydrolytic enzyme functions. Taxonomic identifications of MAGs were similar to the 16S
388 amplicon results, with some differences likely due to different databases queried for the two
389 data types (Fig. S8). We built 36 MAGs, of which 26 were high quality, eight were medium
390 quality, and two were discarded due to redundancy >10% (Table S4). We calculated the relative
391 abundance of each MAG in each treatment community, mapped the functional transcripts to
392 the MAGs, and selected the KOs associated with chitinase or aminopeptidase (proteinase)
393 activity (Fig. 8). In Figure 8, each bubble represents the number of unique MAG contigs that
394 mapped to each KO, identifying 13 chitin metabolism KOs and 20 aminopeptidase-related KOs.
395 MAG_09 (*Caproiciproducens* sp.) had the highest number of functional chitinase-associated
396 KOs, followed by MAG_41 (*Aquitalea* sp.), and MAG_21, MAG_22, and MAG_23 (Order
397 Sphingobacteriales). Protease activity was well-represented across the MAGs, with the highest
398 abundance of aminopeptidase-related KOs associated with MAG_24 (*Phenylobacterium* sp.),
399 followed by MAG_29 (*Shinella sumatrensis*), MAG_33 (*Comamonas acidovorans*), and MAG_30
400 (*Sphingomonas* sp.).

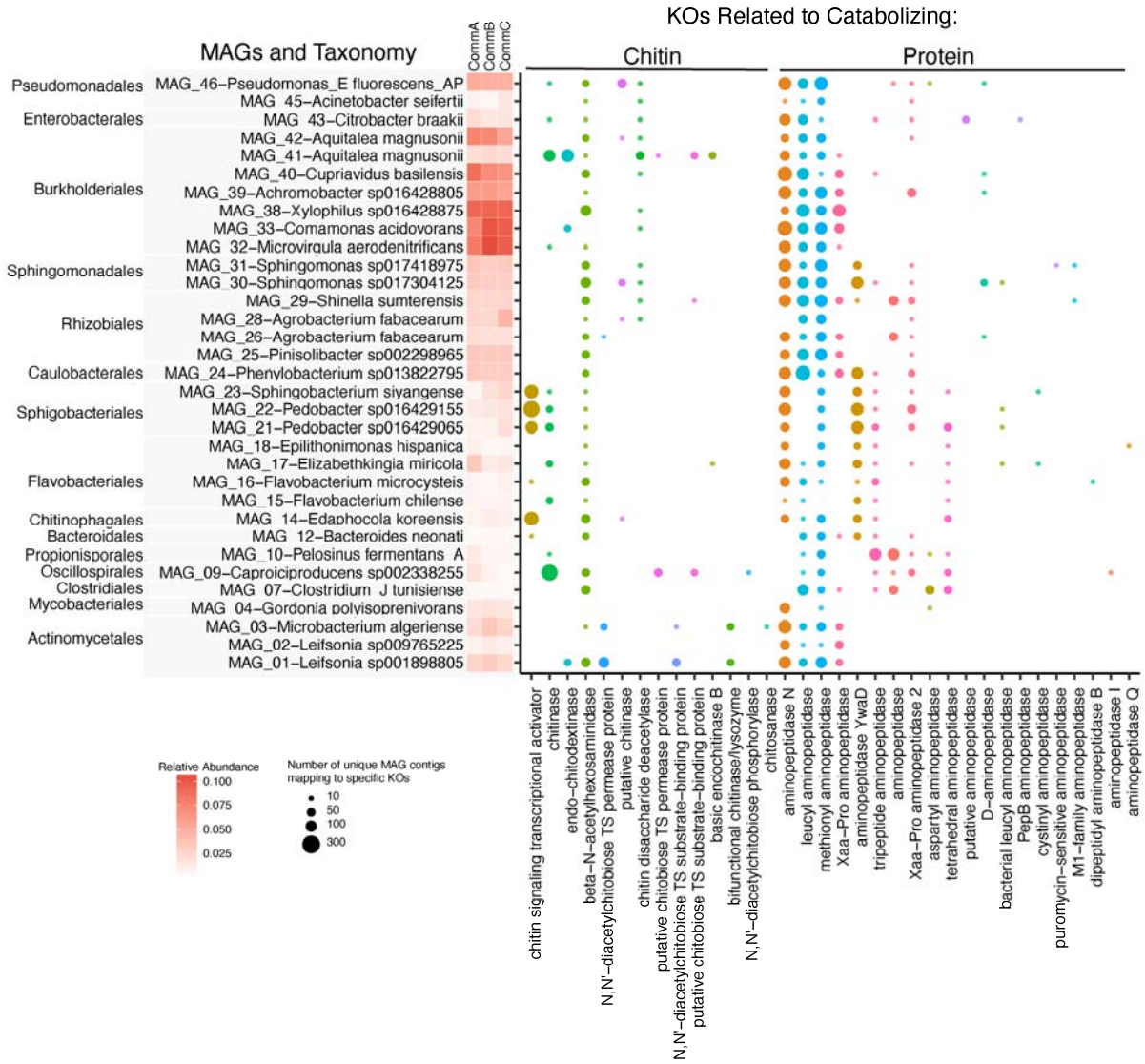

Figure 8. Metagenome assembled genomes (MAGs) enriched in functions related to chitin and protein metabolism. The size of the bubble represents the number of unique MAG contigs mapped to functional transcripts (RNA sequences from the same samples) grouped by KEGG orthology (KO, x-axis) and filtered to include only those KOs associated with targeted hydrolytic enzyme functions (chitin and aminopeptidase metabolizing KOs). The y-axis is ranked by phylogenetic relatedness and shows the MAG identifier along with the associated taxonomy and a heatmap of the relative abundance of each MAG in the three community treatments.

Discussion

Bacterial community functioning influences plant traits

Plants and microbes have been associated for approximately 450 million years (31). Over this vast period, many microbes have evolved beneficial interactions with their hosts; however, our

knowledge of the mechanisms behind mutualistic effects is still limited. In this study, bacterial community function significantly influenced host growth and nutrient acquisition in the pitchers of carnivorous pitcher plants, almost doubling pitcher biomass, and we identified potential functional drivers of these differences. These results addressed our initial question of whether functionally-different bacterial communities have varying effects on host plant traits, where we found positive effects of CommB on pitcher biomass, length, and carbon content. Functional differences among the bacterial community treatments, such as chitinase activity, were correlated with pitcher growth and plant nutrient acquisition. Many studies provide evidence for how the metabolites produced by microbes incite benefits to their host plants, for example, plant growth promoting hormones (17, 32, 33). However, this is the first example to our knowledge, connecting collective microbial community function to host health using metabarcoding, metagenomics, and metatranscriptomics.

This research leveraged a unique model system, with microbes hosted in aquatic microecosystems inside pitcher-shaped leaves, in contrast to classic non-aquatic phyllosphere systems . One might expect that the aquatic pools would have a lower impact on host health than more intimate associations such as root and leaf associated microbial communities. However, the positive effect of bacterial communities on leaf biomass *in planta* in just over eight weeks demonstrates a rapid response to their microbial communities for these slow-growing, long-lived plants. In this experiment, a single pitcher was responsible for nitrogen acquisition for the whole plant, so the other pitchers in the experimental plants were filled with sterile water so could not access N. It is likely that nitrogen was translocated out of the target pitcher to support other pitchers (8, 23), reducing the sensitivity or size of the effect on just the measured target pitchers. These plants generally have low nitrogen content compared to other plants (34), suggesting that even small increases in nitrogen could significantly improve their growth and fitness (34). Additionally, several plant traits were examined, and we found that the percent of carbon and nitrogen in the target pitcher was highly correlated with the second-newest pitcher, which was not inoculated, indicating that nutrient translocation was likely occurring. Our findings demonstrate that functionally different microbial communities can influence host plant health, most likely via the release and supply of nutrients that enhance plant growth and fitness.

Relationship between bacterial composition and function

Recent studies have linked microbially mediated plant benefits to specific taxa. For example, in an experiment with synthetic microbial communities, pathogen suppression in *Arabidopsis* was driven by three specific bacterial taxa (37). In contrast, other studies have observed a community-level effect, such as the positive influence of microbial communities, but not individual strains, on duckweed growth (6, 9, 35). Our study supports the latter situation, as we did not see the presence or absence of specific taxa driving main effects. One possible explanation could be the importance of microbe-microbe interactions, metabolic collaboration in microbial communities is common, making the effects of single taxa less likely (6, 11, 38). Addressing our second question, although we found clear taxonomic and functional differences in our bacterial communities, most ASVs and MAGs were shared across all three communities and the differences were in rare taxa, without specific taxa appearing to drive primary

459 functional differences. In our study, observed differences in hydrolytic enzyme activity and
460 substrate use were likely affected by small differences in relative abundances of functionally
461 important taxa across our communities. Our results indicate that bacterial community functions
462 are not solely determined by composition but, instead, specific combinations of taxa and
463 differential gene expression lead to distinct functional profiles. Corroborating our findings, a
464 2023 study with wild pitcher plants found significant functional differences in the microbial
465 community with modest microbial compositional changes following an experimental
466 manipulation, suggesting that differential gene expression, not composition, drove functional
467 change (38). Similarly, in lake microbial communities, functional differences were only weakly
468 related to taxonomic composition (39). Plants often host high bacterial biodiversity, providing
469 complex habitats and resources that create bacterial niches (40). In pitcher plants, the
470 colonization of pitchers by microbial communities are influenced by factors like season, host
471 characteristics, and nutrient inputs, and these differences in microbial community composition
472 likely have important implications of community function (26, 41, 42). In this study, we
473 demonstrated that relatively small differences in bacterial composition and abundance within
474 pitchers can have significant consequences for nutrient cycling from captured prey supplied to
475 the host plant.
476
477 **Coupling measured bacterial functions with differential gene expression**
478 Our agnostic approach, to examine total gene expression, allowed us to first examine general
479 functional differences across the three bacterial communities. While substantial differences in
480 hydrolytic enzyme activity were observed between bacterial communities after some time *in*
481 *planta*, these did not fully explain the observed benefits to plant biomass and pitcher nutrient
482 acquisition, suggesting a more synergistic, collective community effect rather than the additive
483 effect of transcription of selected genes. Each community exhibited differential transcription of
484 a large number of unique genes, many of which are involved in producing enzymes involved in
485 breaking down complex substrates. Interestingly, despite this untargeted approach, CommB
486 had two chitinase-related KOs among its highest transcribed functions, further supporting this
487 as an important function for liberating nutrients including nitrogen from chitin (43).
488 Additionally, many of the most highly transcribed genes found in CommB mapped to KOs
489 relating to breaking down xylobiose, carnitine, and chitin, indicating this community is efficient
490 at metabolizing complex organic nutrients with probable benefits to the host plant and other
491 members of the microbial community. The catabolism products of these substrates have been
492 found to trigger plant responses, including defense and growth (44, 45). Lastly, while not in the
493 top 20 KO functions, the ACC deaminase gene was significantly higher expressed in CommB.
494 This enzyme plays an influential role in reducing ethylene mediated stress, which can have
495 cascading benefits on growth and development (32). Together, these findings suggest that
496 differential gene expression between microbial communities, due to subtle differences in
497 composition, can contribute to measurable differences in host plant growth.
498
499 **Targeted bacterial functions influence plant traits**
500 Few studies have successfully linked direct enzyme activity with transcriptomics for whole
501 microbial communities. Bacterial communities play pivotal roles in nutrient transformations, so
502 in order to better understand community functional dynamics, we linked bacterial physiology

with hydrolytic enzyme expression to investigate how chitinase and protease activities *in planta* related to differential gene expression for these functions. CommB and C exhibited higher chitinase activity in physiological assays, and CommB also showed significantly higher expression of genes related to chitin degradation in our metatranscriptomic analyses, connecting active enzyme activity to gene expression. In contrast, CommB had lower leucyl aminopeptidase activity measured via a laboratory assay, while differential gene expression identified many genes mapping to various aminopeptidase enzymes expressed in CommB. These results provide evidence that while culture-based physiological assays are valuable, they fail to completely characterize total nutrient cycling activities present in a community. Pairing physiological assays with metatranscriptomics built a clearer picture of the functional activities present in our communities.

The analysis of carbohydrate and amino acid metabolism across the three bacterial communities supports our findings on hydrolytic enzyme activities, revealing distinct organic substrate preferences among the communities. CommB exhibited higher utilization for substrates like N-acetyl glucosamine (GlcNAc) and cellobiose. GlcNAc is a monomer of chitin, chitobiose, or chitotriose and is used for many critical metabolic functions within bacterial cells (46–48), while cellobiose is a metabolic precursor to glucose and interacts with β-glucosidase to yield two glucose molecules used in glycolysis (49). Increased transcription of genes related to metabolizing these substrates provides further evidence that CommB is efficiently cycling diverse nutrients in this community, products which are likely important for not only community cross feeding but for nutrient supply to the host plant. Although it has long been assumed that bacterial community enzyme activity is a key mechanism in pitcher plant nutrient acquisition(23, 50), our results are the first to directly measure and provide evidence for this mechanism.

Conclusion

In this controlled study, plant growth was enhanced by the collective function of a specific bacterial community. The most growth was observed in pitchers hosting a bacterial community with high chitinase activity and high differential expression of genes related to nutrient cycling, supporting the release of nutrients for uptake by the host plant. We characterized collective community composition and function using a suite of complementary approaches that highlighted the complexity and dynamics of plant-microbe interactions and the role microbial communities can play in host health and growth. The benefits of plant-microbe interactions to host productivity are likely often not driven by a single functional parameter, nor a single taxon expressing a gene encoding a specifically useful function. This bacterial community analysis suggests that measurable functional traits can identify relevant bacterial effects in phyllosphere communities. Identification of these relationships contribute to increased knowledge of the effects of bacterial communities on plant traits and can inform other systems with applications in agriculture, conservation, and restoration.

Methods

Experimental design

547 Mature *Sarracenia purpurea* greenhouse plants (donated by T. Miller, FSU) were surface
548 sterilized and repotted into autoclaved media (7 parts milled sphagnum peat: 3 parts sand) and
549 bleach-sterilized pots. Plant surface sterilization consisted of washing the leaves and roots in
550 distilled water prior to soaking in 1% hydrogen peroxide for 15 minutes (repeated 3X). Plants
551 were transferred into clean plant growth chambers (Hoffman Mfg. Inc. Corvallis, OR USA, SG2-
552 22) and allowed to acclimatize for 12 weeks prior to the start of the experiment. Care was taken
553 to keep the plants, pots, and all contact with the growth chambers as sterile as possible,
554 however chambers were supplied with f ambient unfiltered air through their vents and when
555 the chamber doors were open. The chambers were configured with a diel light and
556 temperature cycle, 14-hour photoperiod (Photosynthetic photon flux density (PPFD)= 62 µmol
557 m^{-2} s^{-1}) at 31 °C and 10 hours dark at 17 °C, with relative humidity at 70%. Additional
558 temperature probes were added to each chamber to monitor chamber conditions.
559
560 The three distinct bacterial communities (CommA, CommB, and CommC) used for inoculation
561 were previously collected from wild *S. purpurea* pitcher plants (51). These communities were
562 selected from the ten microcosm communities used by Bittleston et al. 2018 (CommA=M01,
563 CommB=M06, CommC=M09). All ten communities from that study were reconstituted from
564 cryogenic culture and grown in the lab using acidified cricket media (ACM) with 1:1 serial
565 transfers into fresh media every 72 hours for several months. Cricket media was used to
566 establish the bacterial communities and was prepared by acidifying (pH=5.6, 1.0M HCl) ground
567 food-grade house cricket media (3g/L H_2O Thailand Unique Inc.), then autoclaving. The three
568 communities (CommA, CommB, CommC) were selected based on their differences in chitinase
569 and protease activity (Fig. 2). In addition to three experimental bacterial communities, two
570 experimental controls were ACM only and sterile deionized water only. Both controls contained
571 no bacterial cultures, the ACM control was used to test effects of nutrient media without any
572 bacteria on plants. The water control examined the effect of sterile ACM media with no
573 bacteria.
574
575 Ten individual pitcher plants were randomly assigned to each bacterial treatment group and six
576 to each control group, for a total of 42 individual plants. On day 0, on each plant, one new,
577 unopened pitcher was manually opened using sterile gloved hands and carefully inoculated
578 with a bacterial community culture or control treatments until each pitcher was 3/4ths full. For
579 example, if a pitcher held 8 mL when 3/4ths full, it received 8 mL sterile ACM and 0.8 mL
580 bacterial community culture. Due to varying pitcher sizes, some smaller pitchers received lower
581 volumes in the same media:culture ratio. The single pitcher on each plant that received one of
582 the five treatments was the target pitcher (pitcher 1). All other pitchers on each plant received
583 sterile water for the duration of the experiment. For some plant trait measurements, data were
584 also collected on the second-newest pitcher (pitcher 2). We found no statistical differences in
585 the optical density or the bacterial cell concentration (from CFU counts) between our three
586 cultures prior to inoculation.
587
588 Because plants did not all have new, unopened pitchers on the same week, new plants were
589 added to the experiment in stages, once a week for 5 weeks until all plants had been
590 inoculated. To ensure there was no effect of this staggered addition of plants, plants were

591 assigned to treatment groups randomly and sample analysis was based on time after
592 inoculation, not date. The cultures for the three bacterial communities were maintained (as
593 noted above) in the lab and added each week to the appropriate plants. There was no change
594 in bacterial community composition in these cultures, and we found that community
595 composition of samples within the same treatment, but added on different weeks, had very
596 tight clustering 7 days after inoculation, regardless of date added. Every 2 days, distilled water
597 was added to the trays under the pots, to prevent splashing and contamination into pitchers.
598 Each week, the plants were rearranged within the chamber and rotated according to a
599 randomization map created using a random number generator.
600
601 **Sample collection**
602 Samples were collected weekly, starting the day after inoculation (day 1) 4.0 mL was collected
603 from each leaf using sterile technique. This sample was then aliquoted, 1.5 mL was frozen in
604 sterile screw cap tubes for amplicon sequencing, 750 µL was frozen in cryotubes in liquid
605 nitrogen for metagenomic/metatranscriptomic analysis, 750 µL was mixed with 750 µL 80%
606 sterile glycerol and frozen in screw cap tubes for culture preservation. All preserved samples
607 were stored at -80 °C until nucleic acid extraction. The remaining 1.0 mL was used in the
608 microbial physiological assays described below. The full 4.0 mL was not removed from very
609 small pitchers on day 7 due to limited volumes, but in all cases pitcher size increased very
610 quickly in the first week and full samples were collected at future samplings. In all plants,
611 sample volume (4.0 mL) was replaced with sterile cricket media as a weekly food source, and an
612 additional 2 mL sterile water added to pitcher 1 to replace evaporated fluid (total added liquid
613 each week to all plants = 6.0 mL). There was some damage that occurred to some pitchers
614 during the course of the experiment, plants 25 (CommB), 44 (CommB), 51 (CommC), 9
615 (CommC), and 29 (CommA) were removed from all analyses.
616
617 **Bacterial Physiological Assays**
618 Chitinase and protease activities were quantified weekly on a sample from each treatment
619 pitcher using fluorometric assays in black 96-well microplates (24, 52). Fluorescence emission
620 was measured every five minutes for one hour using a microplate reader (Biotek Synergy Mx
621 Multi-Mode Microplate Reader). Of three types of chitinases found in the *S. purpurea* pitchers
622 communities, chitobiosidase activity was selected for quantification because preliminary data
623 showed higher activity potential than β-N-acetylglucosaminidase and triacetyl chitotriosidase.
624 Chitobiosidase (hereafter chitinase) activity was measured using 200 µL of sample (culture or
625 pitcher fluid) and 50 µL of substrate (0.86 mM 4-Methylumbelliferyl N, N′-diacetyl-β-D-
626 chitobioside in 50 mM Tris-HCl pH 8.0 with 0.1% bovine serum albumin) as described in (24).
627 Standards of 4-methylumbelliferone were made from 0 to 1 µM concentrations and read at 360
628 nm excitation and 420 nm emission. L-amino peptidase (protease) activity was measured using
629 50 µL of sample added to 25 µL of 50 mM Tris-HCl pH 7.5 and 75 µL of substrate (2 mM L-
630 leucine-7-amido-4-methylcoumarin hydrochloride in nanopure water). Standards of 7-amino-4-
631 methylcoumarin were made from 0 to 1000 nM concentrations and read at 380 nm excitation
632 and 460 nm emission. Using the standard curves for each assay, fluorometric readings were
633 converted to product concentrations and plotted through time to get the linear enzymatic rate
634 for each sample (24).

635
636 The "functional fingerprint" for each bacterial community was measured by examining the
637 community's capacity to use 31 carbon substrates. These measurements were conducted on
638 the first and last day of the experiment (day 1 and 55) using Biolog EcoPlates™. EcoPlates were
639 inoculated with 100 µL of diluted sample (1:40 in sterile DI water) and allowed to incubate in
640 the dark at room temperature, absorbance readings were collected every 24 hours until a
641 maximum color change had been observed (72 hours). The changes in color were quantified by
642 reading the absorbance using a plate reader (above) at a wavelength of 590 nm. Water was
643 used as a control blank and subtracted from each absorbance reading prior to analysis.
644 Experimental controls were removed from the EcoPlate analysis. After an initial analysis,
645 extreme outliers at day 55 were removed the EcoPlate analysis, including plants 34 and 15 from
646 CommA, 27 from CommB, and 28, 21, and 41 from CommC.
647
648 Bacterial community growth metrics (maximum growth rate, doubling time, carrying capacity)
649 were measured using optical density at 590 nm for bacterial communities prior to inoculation
650 (Day 0) and from pitcher fluid samples at the end of the experiment (day 55). Bacterial cultures
651 and pitcher fluid samples (2 µL) were added to 198 µL R2A media in a clear flat bottom 96 well
652 plate (53). Plates were incubated in a plate reader (Tecan Spark) at 18 °C and absorbance was
653 measured every 30 minutes for 48 hours. Bacterial growth metrics were analyzed using the R
654 growthcurver package (54). The microbial community respiration was measured (as CO_2
655 produced) for both the bacterial cultures prior to the experiment (Day 0) and for pitcher fluid
656 samples at the end of the experiment (day 55), using the MicroResp system (55). Samples were
657 added to a sterile deep well plate (250 µL) along with 250 µL acidified cricket media. The plate
658 was fitted with a silicon mat with small holes and an indicator plate, both plates were clamped
659 into the MicroResp apparatus and incubated in the dark at room temperature. The indicator
660 plate contains a pH sensitive dye (cresol red 12.5 ppm, wt/wt) that shifts from magenta to
661 yellow in the presence of carbon dioxide. The absorbance at 570 nm was measured prior to
662 incubation, and consecutively after 6, 24, and 48 hours. Carbon dioxide concentrations were
663 calculated using a standard curve created by incubating an indicator medium with a series of
664 known carbon dioxide concentrations. Respiration rates were calculated for the first 24 hours
665 of respiration as a change in the CO_2 produced over the first 24 hours.
666
667 **Plant functional traits**
668 Pitcher morphological traits (56), including length, width, and opening aperture (56) were
669 measured weekly for eight weeks (day 0, 7, 14, 21, 28, 35, 42, 49, 55). For each plant, the
670 number of mature leaves was recorded at the beginning and end of the experiment. The length
671 of each pitcher (rhizome to tip) was measured with a flexible tape (cm) and the pitcher
672 diameter (at widest point), and aperture of the pitcher, will be measured with digital calipers
673 (mm). Tools were carefully sanitized with 70% ethanol between each measurement. At the end
674 of eight weeks, two pitchers were cut at the base for biomass measurements, the target pitcher
675 (pitcher one) and a secondary mature pitcher (second-oldest pitcher, pitcher two). Biomass was
676 measured by first taking a wet mass, drying the plant tissue at 65 °C for 72 hours, then
677 recording the dry mass. Plant tissue was homogenized in a spice grinder, for a subset of plants
678 (n= 15), we also harvested the remaining pitchers, roots, and rhizomes to investigate plant level

679 differences in biomass and C: N for plants in different treatment groups. Whole plant (pitcher,
680 root, rhizome) samples were collected for nutrient content analysis at the end of the
681 experiment (three whole plants from each treatment (n=15) and the two main pitchers from
682 the remaining plants). Plant tissue was dried at 65 °C for 72 hours and stored in the dark at
683 room temperature until samples were homogenized. Powdered samples were analyzed using a
684 CN elemental analysis (Flash EA1112), the proportion of carbon and nitrogen for each tissue
685 sample was calculated using the mass of the nutrient divided by the mass of the ground
686 sample.
687
688 Photosynthetic rates (µmol CO_2 m^{-2} s^{-1}) of the target pitcher (pitcher one) and secondary
689 mature pitcher (pitcher two) were measured separately at the end of the experiment (day 55)
690 using a LICOR-6400 photosynthesis system (LICOR Inc., Lincoln, NE) and leaf chamber
691 fluorometer (LCF 6400-40). Measurements were taken between 1000 and 1300 h on plants
692 removed from the growth chambers, pitchers were filled with distilled water.
693 Photosynthetically active radiation (PAR) was set to 1200 µmol photons m^{-2} s^{-1} for 5 min. A
694 subset of plants (three plants from each of the five treatments, n=15) had photosynthetic rates
695 measured on the youngest mature pitcher on each plant, prior to inoculation and addition to
696 the experiment.
697
698 The maximum quantum efficiency of photosystem II photochemistry (F_v/F_m)(57) was measured
699 once daily for one week, then weekly for 8 weeks. A portable multimode chlorophyll
700 fluorometer (Opti-Sciences) was used to measure the maximum quantum yield (F_v/F_m) of
701 chlorophyll fluorescence after a 25-minute period of dark acclimation using plastic leaf
702 clips(34). The fiber optic cable was wiped with 70% ethanol between each plant and the plastic
703 leaf clips were sanitized with 10% bleach, rinsed with DI water, and allowed to air dry after each
704 measurement.
705
706 Many plant traits were measured (leaf length, width, aperture, biomass, photosynthetic
707 efficiency, photosynthetic rate, pitcher carbon, pitcher nitrogen, total number of leaves, new
708 leaves). The collinearity in the response variables was assessed using a principal components
709 analysis (PCA) on scaled data, dimension 1 explaining 77.1% of the variance and dimension 2
710 explaining 7.9% (Fig. S9). Along dimension 1, pitcher morphological measures (length, width,
711 aperture, biomass) were tightly correlated with each other. Pitcher dry biomass was selected as
712 the representative measure of plant size. Pitcher nitrogen and carbon content were selected as
713 measures of nutrient assimilation (Fig. S9).
714
715 **16S rRNA sequencing and analysis**
716 To characterize bacterial community composition, DNA was extracted from all samples
717 (CommA, CommB, CommC, ACM & water controls, on day 8, 15, 22, 29, 36, 43, 50, 55, n=310)
718 using the DNAdvance Genomic DNA Isolation Kit (Beckman Coulter A48705). Samples (750 µL)
719 were bead beaten in lysis buffer at 2400 RPM for 10 min, and then incubated at 55 °C shaking
720 (150 RPM) overnight before proceeding with the extraction (halving all the reagents but
721 following the protocol per the manufacturer's directions), each 96-well plate included one
722 negative control. DNA was quantified using AccuClear Ultra HS dsDNA kit (Biotium #31028). 16S

723 rRNA gene amplification and library preparation and sequencing was conducted by the
724 Environmental Sample Preparation and Sequencing Facility at Argonne National Laboratory on
725 a 151 bp x 12 bp x 151 bp Illumina MiSeq run targeting the V4 region of 16S rRNA using the
726 515F and 806R primers (58).
727
728 The 16S rRNA gene sequences were processed in QIIME2 (version 2022.8), demultiplexed using
729 no-golay error correction and quality filtered to remove reads with a mean score less than 20,
730 and trimmed to the sequence length of 150 base pairs. The DADA2 (74) module was used to
731 denoise sequences and generate amplicon sequence variants (ASVs) (59, 60). Taxonomy was
732 assigned using the classify-sklearn method which is a Native Bayes classifier, and a pre-trained
733 classifier made with Silva v. 138 database containing 99% amplicon sequence variants (ASVs)
734 from 515F/806R region (61). The phylogenetic tree was built using multiple-sequence
735 alignment via SEPTT and phylogenetic reconstruction via FastTree, both via a QIIME2 plugin (62,
736 63). Taxonomy and ASV tables were migrated to R for further analysis and visualization using
737 qiime2R, picante, and phyloseq (64–66).
738
739 Across 316 samples (310 pitcher fluid samples and 5 negative controls) *DADA2* generated 2633
740 ASVs. Contaminant ASVs were identified and discarded using the *decontam* R package (67), the
741 *decontam* method "prevalence" was used which identified ASVs based on their presence and
742 abundance in our negative controls. Data was quality filtered to remove non-prokaryotic ASVs
743 and ASVs classified as mitochondria or chloroplasts, and only include observations with at least
744 10 sequences and samples with at least 1000 sequences, resulting in 310 pitcher fluid samples
745 (day 8 through day 55) with a cumulative 1036 distinct ASVs, with 25317 mean reads per
746 sample (min reads/sample = 1669; max reads/sample= 57927). Samples were rarified down to
747 1669 reads, resulting in 310 samples with 1036 ASVs. A negative binomial model was built using
748 the *brms* package to investigate the effect of a treatment group on alpha diversity (68).
749
750 For ASV-level differential abundance explained by the treatment groups, an analysis of
751 compositions of microbiomes with bias correction (*ANCOMBC2*) was used, this is a Bayesian
752 statistical approach that accounts for sampling fraction, normalizes the read counts, and
753 controls for false discovery rates (fdr) (28). Quality controlled but unrarefied ASV counts were
754 analyzed using the *ANCOMBC* function, adjusted p-value method was set to fdr, prevalence
755 (prv_cut) was set to 0.3, the level of significance (alpha) was set to 0.05, pairwise directional
756 test (pairwise) was set to TRUE, with the rest of the parameters left as default. Significantly
757 differentially abundant ASVs were identified across the treatment groups and through time.
758
759 **Metagenomic and metatranscriptomic sequencing and analysis**
760 The pitcher fluid from three of the 10 pitchers in each treatment group were selected from
761 three time points (3 plants x 3 treatments x 3 timepoints (day 1, 22, 55), n=27) for simultaneous
762 DNA/RNA extractions for metagenomic and metatranscriptomic sequencing using the Qiagen
763 AllPrep Bacteria DNA/RNA/Protein Kit (Cat 47054), according to manufacturer directions.
764 Briefly, flash frozen samples were thawed and pelleted, pellets were resuspended in lysis
765 solution and bead beat for 10 minutes at 2400 RPM after which 350 µL of lysate was
766 transferred to a spin column were the DNA was collected in the column and the flow through

767 was further processed for RNA extraction. Samples were eluted in nuclease free water and
768 stored at -20°C until quantification and library preparation. Nucleic acids were quantified using
769 a fluorometer (Qubit, Invitrogen). Libraries were prepared for the full 27 RNA samples using
770 NEBNext rRNA Depletion Kit (NEB#E7850) and NEBNext Ultra II Directional RNA library prep kit
771 for Illumina (NEB#E7760) using manufacturer protocols. Metagenomic libraries (DNA) were
772 prepared for a subset of these samples (3 plants x 3 treatments x 2 timepoints (day 1, 55),
773 n=18) using NEBNext Ultra II FS DNA library prep kit for Illumina (NEB#78055). Sequencing was
774 done on a NovaSeq partial lane to a sequencing depth of 55 Gb per library at Novogene Co.
775 (Sacramento, CA USA).
776
777 Shotgun metagenomic and metatranscriptomic sequences were processed on BSU's Borah
778 cluster. Adapters and low quality sequences were trimmed using Trimmomatic (0.39) with the
779 following settings: SLIDINGWINDOW:4:20 MINLEN:25 ILLUMINACLIP:TruSeq3-PE.fa:2:40:15
780 based on the FastQC (v0.12.1) and viewed with MultiQC (v1.6) quality reports (69–71).
781 Metatranscriptomic sequences were further processed to remove ribosomal RNA using the
782 default settings (-t 4, -l 150, -e rrna) in Ribodetector (72). Two co-assemblies were produced
783 (metagenomic and metatranscriptomic) using MEGAHIT (v1.2.9) (73, 74).
784
785 For the metagenomic analysis, the "sketch", "gather", and "tax annotate" functions within
786 sourmash (version 4.8.2) (75) using kmer=31 were used to assign and quantify taxonomy using
787 the full GTDB database (R08-RS214 403k) (76). Contigs in the coassembly and paired-end reads
788 were binned using MAXBIN2 (2.2.7), CONCOCT (1.1.0), and Metabat2 (2.12.1), consensus bins
789 were produced using DASTool (1.1.6) (77–80). Completeness and contamination of each
790 metagenome assembled genome (MAG) were calculated using the presence of single-copy
791 marker genes with CHECKM2 v.1.0.11 (81). Comparisons and dereplication of MAGs employed
792 dREP v.2.2.1 (82). Taxonomy was assigned to the quality-controlled MAGs using the full GTDB
793 database within sourmash. Bins were quality ranked according to their completeness and
794 contamination (>90% completion, <5% redundancy), medium quality (>50% completion, <10%
795 redundancy), low quality (<50% completion, <10% redundancy), or discarded (>10%
796 redundancy) (83, 84). The abundance of each MAG in each treatment was calculated by first
797 building an index for each MAG using the `index` function in bwa (85), using bwa and samtools
798 (86) to align the individual forward and reverse sample reads to each MAG. The phylogentic
799 tree for the MAGs was built by first extracting the marker genes from each MAG using the
800 `ineage_wf' and `qa' tools from CHECKM2 (81) and then multiple sequence alignment with
801 MAFFT (62). The phylogenetic tree was built with IQ-Tree (87) and parsed in R. Predicted gene
802 sequences from the metatranscriptomic samples were mapped to a custom database built with
803 the MAGs, and then used blastn (88) to quantify the number of contigs in each MAG that
804 matched with each predicted gene.
805
806 For metatranscriptomic analyses, we used SeqKit (89) and VSEARCH (90) to look at the quality
807 of coassembly before and after chimera removal. We removed 23 contigs that surpassed the
808 50,000 base pair threshold. Open reading frames (ORFs) were predicted using Prodigal (v2.6.3)
809 (91). We used CDHIT to remove redundancy in our predicted proteins by clustering transcript.
810 Transcript abundance quantification was done in Kallisto (v1.9.0) and resulted in transcripts per

811 million (TPM) and counts for each transcript and sample (92). KOFAMSCAN (1.3.0) was used to
812 bin ORFs into KOs using the full KEGG database (93).
813
814 Differential transcript abundance was quantified using *Dream* within the *variancePartition*
815 package (94) with treatment set as a fixed effect and plant ID set as a random intercept to
816 account for repeated measures across three time points. The dream model was used to
817 estimate weights using our pre-defined linear mixed model and then fit the model using the
818 Satterthwaite approximation. The coefficient table was filtered down to those z-scores greater
819 than or equal to the critical value of 1.645 resulting in those genes that are differentially
820 expressed across our treatments. Within this model, contrasts were created to compare the
821 expression levels of genes in each community treatment against the average of the other two:
822 CommA vs (CommB + CommC)/2, CommB vs (CommA + CommC)/2, CommC vs (CommA +
823 CommB)/2.
824
825 **Statistical analyses**
826 All statistical analyses were conducted in R version 4.2.2 (95). Alpha diversity metrics (Hill
827 Number 1) were calculated using the *vegan* package (96) and additional processing used
828 *tidyverse* and *janitor* (97–99). For ASV-level differential abundance explained by the treatment
829 groups, we used *ANCOMBC* (ancombc2(data = tse, assay_name = "counts", tax_level = NULL,
830 fix_formula = "treatment", rand_formula = "(1 | week)", p_adj_method = "fdr", pseudo_sens =
831 TRUE, prv_cut = 0.3, group="treatment", alpha = 0.05, n_cl = 3, verbose = TRUE, global = TRUE,
832 pairwise = TRUE)) (28). Significantly differentially abundant ASVs were visualized with box plots
833 and a heatmap (100) by transforming the normalized reads: (log2(read count+0.5)).
834
835 Community similarity in ASVs and EcoPlate carbon substrate use among samples in each
836 treatment group was determined using the vegan package (96). Compositional differences
837 (beta diversity) and changes across the three bacterial community treatments from day 8 to 55
838 were assessed using phylogenetic methods, unweighted UniFrac (101). Mantel tests (96)
839 assessed correlations between bacterial composition and hydrolytic enzyme activity or pitcher
840 biomass. To visualize the similarity in EcoPlate carbon substrate use among samples and
841 treatments, a *metaMDS* analysis with Bray-Curtis distance at two dimensions (k=2) was utilized.
842 In both cases, non-metric multidimensional scaling (NMDS, (96)) visualized the dissimilarities
843 calculated between each pitcher fluid sample. A non-parametric multivariate analysis of
844 variance test (*PERMANOVA*, *adonis2* function, by="margin") was used to assess any differences
845 between treatments, and *pairwise adonis* was used to assess the effects of treatment and time,
846 while accounting for repeated measures for each pitcher (96). Dispersion, or the homogeneity
847 in dispersion between treatments, was calculated using the *betadisper* function (permutations
848 compared using a post-hoc Tukey test, (96).
849
850 Metatranscriptomic statistical analyses began with a matrix of filtered genes (length>500bp),
851 samples were normalized using the *calcNormFactors* function in the *variancePartition* package
852 (1.28.9). Differential transcript abundance was quantified using *Dream* within the
853 *variancePartition* package (94). In order to link specific taxa to differentially expressed

854 functions, significantly differentially abundant contigs were mapped to the MAGs using a
855 custom database built from the MAG contigs and *BLAST* (2.14.0) (88).
856
857 To isolate the impact of functionally distinct bacterial communities on plant traits (after 8
858 weeks *in planta*, Questions 1 and 2), we developed Bayesian generalized linear mixed models
859 (GLMMs) using variables based on the causal assumptions of directed acyclic graphs (DAGs).
860 Directed acyclic graphs help identify which observed and unobserved variables to condition
861 upon to remove non-causal associations between variables and isolate mechanisms of interest,
862 under the assumption that the depicted pathways between variables in a research design are
863 accurate (102, 103) Therefore, GLMMs contained a variable set designed to isolate the effects
864 of treatment and enzymatic activity from the other unspecified and unrecorded impacts of our
865 bacterial treatments (Fig. S1) (68). Pitcher biomass was selected to represent the
866 morphometrics and growth, along with leaf nitrogen content representing leaf nutrient
867 acquisition. To consider non-independence of repeated measures of pitchers over time, models
868 included a random intercept for pitcher identity. Other random effects like inoculation date and
869 initial pitcher volume were not accounted for in the model but controlled for by the
870 randomized design.
871
872 Bayesian hierarchical models using a gamma (log-link) GLM were fitted using the *brms* package
873 (68, 104) and visualized using *bayesplot*, *ggeffects*, and *tidybayes* (105–107). Bayesian GLMs are
874 robust to small sample size and outliers, and the gamma distribution best fits the data
875 generating processes (108, 109). The continuous predictor variables were standardized and
876 mean centered using the *standardize* package (108). In all models that contained the treatment
877 group as a predictor, we set ACM as the baseline, to compare the effects to pitchers with food
878 but no inoculated bacteria. Default uninformative priors were used, convergence and mixing of
879 chains and unimodality in posterior predictions were visually assessed, and all R-hat values
880 were close to 1.0 (68). The model fit was evaluated using the posterior predictive check
881 function in *brms* (68).
882
883 **Acknowledgements**
884 We would like to acknowledge Stacey Pedraza for help with processing samples, the late Bill
885 Freutel and other members of the Earth, Wind, Fire Lab for use of lab space, Dr. Linda Reynard
886 for FLASH assistance, and Franco Nero and Jacob Heil for help with experiments. We offer our
887 gratitude to Dr. Allison Simler-Williamson and the Ecological Statistics community at BSU for
888 valuable feedback. We would like to thank Dr. Ben Baiser and Dr. Zac Freedman for helpful
889 suggestions and feedback on the final manuscript.
890
891 **Data Availability Statement**
892 Scripts and data associated with this manuscript are available at:
893 https://github.com/jessibernardin/microbial-function-plant_trait. The raw reads for 16S rRNA
894 amplicon sequencing, raw reads for whole genome shotgun sequencing, whole genome
895 metatranscriptomic sequencing, and nucleotide sequences of MAGs have been deposited in the
896 National Center for Biotechnology Information (NCBI) under the project number
897 PRJNA1028624.

898
899 **Competing Interests**
900 Authors have no competing interests to declare.
901
902 **Funding Statement**
903 JRB, LSB and EBY were supported with funding from the National Science Foundation through
904 an Understanding the Rules of Life-Microbiome Theory and Mechanisms 2 collaborative grant
905 (award #2025250 to LSB and award # 2025337 to EBY). LSB was also funded by an award from
906 the Simons Foundation, LS-ECIAMEE-00001638.
907
908 **References**
909 1. Vandenkoornhuyse P, Quaiser A, Duhamel M, Le Van A, Dufresne A. 2015. The
910 importance of the microbiome of the plant holobiont. New Phytologist 206:1196–1206.

911 2. Simon J-C, Marchesi JR, Mougel C, Selosse M-A. 2019. Host-microbiota interactions: from
912 holobiont theory to analysis. Microbiome 7:5.

913 3. Stone B, Weingarten E, Jackson C. 2018. The role of the phyllosphere microbiome in plant
914 health and function 1:1–24.

915 4. Liu H, Brettell LE, Singh B. 2020. Linking the Phyllosphere Microbiome to Plant Health.
916 Trends in Plant Science 25:841–844.

917 5. Trivedi P, Leach JE, Tringe SG, Sa T, Singh BK. 2020. Plant–microbiome interactions: from
918 community assembly to plant health. Nat Rev Microbiol https://doi.org/10.1038/s41579-
919 020-0412-1.

920 6. Mehlferber EC, Debray R, Conover AE, Sherman JK, Kaulbach G, Reed R, McCue KF, Ferrel
921 JE, Khanna R, Koskella B. 2023. Phyllosphere microbial associations improve plant
922 reproductive success. Front Plant Sci 14.

923 7. Delmotte N, Knief C, Chaffron S, Innerebner G, Roschitzki B, Schlapbach R, von Mering C,
924 Vorholt JA. 2009. Community proteogenomics reveals insights into the physiology of
925 phyllosphere bacteria. Proceedings of the National Academy of Sciences 106:16428–
926 16433.

927 8. Vorholt JA. 2012. Microbial life in the phyllosphere. Nat Rev Microbiol 10:828–840.

928 9. Flores-Núñez V, Camarena-Pozos D, Chávez Gonzalez J, Alcalde-Vázquez R, Vázquez-
929 Sánchez M, Hernandez-Melgar A, Xool-Tamayo J, Moreno-Ulloa A, Partida Martinez L.
930 2023. Synthetic Communities Increase Microbial Diversity and Productivity of Agave
931 tequilana Plants in the Field. Phytobiomes Journal 7.

932 10. Holland MA. 2011. Nitrogen: Give and Take from Phylloplane Microbes, p. 215–230. *In*
933 Ecological Aspects of Nitrogen Metabolism in Plants. John Wiley & Sons, Ltd.

934 11. Kende H, Zeevaart J. 1997. The Five "Classical" Plant Hormones. Plant Cell 9:1197–1210.

935 12. MacMillan J. 2001. Occurrence of Gibberellins in Vascular Plants, Fungi, and Bacteria. J
936 Plant Growth Regul 20:387–442.

937 13. Spaepen S, Vanderleyden J, Remans R. 2007. Indole-3-acetic acid in microbial and
938 microorganism-plant signaling. FEMS Microbiol Rev 31:425–448.

939 14. Spaepen S. 2015. Plant Hormones Produced by Microbes, p. 247–256. *In* Lugtenberg, B
940 (ed.), Principles of Plant-Microbe Interactions: Microbes for Sustainable Agriculture.
941 Springer International Publishing, Cham.

942 15. Lievens L, Pollier J, Goossens A, Beyaert R, Staal J. 2017. Abscisic Acid as Pathogen
943 Effector and Immune Regulator. Front Plant Sci 8:587.

944 16. Porter SS, Bantay R, Friel CA, Garoutte A, Gdanetz K, Ibarreta K, Moore BM, Shetty P, Siler
945 E, Friesen ML. 2020. Beneficial microbes ameliorate abiotic and biotic sources of stress
946 on plants. Funct Ecol 34:2075–2086.

947 17. Aziz U, Rehmani MS, Wang L, Luo X, Xian B, Wei S, Wang G, Shu K. 2021. Toward a
948 Molecular Understanding of Rhizosphere, Phyllosphere, and Spermosphere Interactions
949 in Plant Growth and Stress Response. Critical Reviews in Plant Sciences 40:479–500.

950 18. Bradshaw WE, Creelman RA. 1984. Mutualism between the Carnivorous Purple Pitcher
951 Plant and its Inhabitants. The American Midland Naturalist 112:294–304.

952 19. Givnish TJ, Burkhardt EL, Happel RE, Weintraub JD. 1984. Carnivory in the Bromeliad
953 Brocchinia reducta, with a Cost/Benefit Model for the General Restriction of Carnivorous
954 Plants to Sunny, Moist, Nutrient-Poor Habitats. The American Naturalist 124:479–497.

955 20. Heard SB. 1998. Capture Rates of Invertebrate Prey by the Pitcher Plant, Sarracenia
956 purpurea L. The American Midland Naturalist 139:79–89.

957 21. Miller TE, Horth L, Reeves RH. 2002. Trophic interactions in the phytotelmata
958 communities of the Pitcher Plant, Sarracenia purpurea. Community Ecology 3:109–116.

959 22. Gallie DR, Chang SC. 1997. Signal Transduction in the Carnivorous Plant Sarracenia
960 purpurea (Regulation of Secretory Hydrolase Expression during Development and in
961 Response to Resources). Plant Physiology 115:1461–1471.

962 23. Butler JL, Gotelli NJ, Ellison AM. 2008. Linking the brown and green: nutrient
963 transformation and fate in the *Sarracenia* microecosystem. Ecology 89:898–904.

964 24. Young EB, Sielicki J, Grothjan JJ. 2018. Regulation of hydrolytic enzyme activity in aquatic
965 microbial communities hosted by carnivorous pitcher plants. Microb Ecol 76:885–898.

966 25. Butler JL, Ellison AM. 2007. Nitrogen cycling dynamics in the carnivorous northern pitcher
967 plant, Sarracenia purpurea. Functional Ecology 21:835–843.

968 26. Bittleston LS, Wolock CJ, Yahya BE, Chan XY, Chan KG, Pierce NE, Pringle A. 2018.
969 Convergence between the microcosms of Southeast Asian and North American pitcher
970 plants. eLife 7.

971 27. Karagatzides JD, Butler JL, Ellison AM. 2009. The Pitcher Plant Sarracenia purpurea Can
972 Directly Acquire Organic Nitrogen and Short-Circuit the Inorganic Nitrogen Cycle. PLoS
973 ONE 4:e6164.

974 28. Lin H, Peddada SD. 2020. Analysis of compositions of microbiomes with bias correction.
975 1. Nat Commun 11:3514.

976 29. Feng Y-S, Chen P-C, Wen F-S, Hsiao W-Y, Lee C-M. 2008. Nitrile hydratase from
977 *Mesorhizobium* sp. F28 and its potential for nitrile biotransformation. Process
978 Biochemistry 43:1391–1397.

979 30. Kanamori T, Kanou N, Atomi H, Imanaka T. 2004. Enzymatic Characterization of a
980 Prokaryotic Urea Carboxylase. Journal of Bacteriology 186:2532–2539.

981 31. Hassani MA, Durán P, Hacquard S. 2018. Microbial interactions within the plant
982 holobiont. Microbiome 6:58.

983 32. Herpell JB, Alickovic A, Diallo B, Schindler F, Weckwerth W. 2023. Phyllosphere symbiont
984 promotes plant growth through ACC deaminase production. ISME J 17:1267–1277.

985 33. Jahandideh Mahjenabadi VA, Sepehri M, Rahmani H, Zarei M, Ronaghi A, Taghavi SM,
986 Shamshiripour M. 2020. Role of Dominant Phyllosphere Bacteria with Plant Growth–
987 Promoting Characteristics on Growth and Nutrition of Maize (Zea mays L.). Journal of Soil
988 Science and Plant Nutrition 20.

989 34. Bott T, Meyer GA, Young EB. 2008. Nutrient limitation and morphological plasticity of the
990 carnivorous pitcher plant Sarracenia purpurea in contrasting wetland environments. New
991 Phytologist 180:631–641.

992 35. Laurich Jason R., Lash Emma, O'Brien Anna M., Pogoutse Oxana, Frederickson Megan E.
993 2024. Community interactions among microbes give rise to host-microbiome mutualisms
994 in an aquatic plant. mBio 15:e00972-24.

995 36. Christensen BB, Haagensen JAJ, Heydorn A, Molin S. 2002. Metabolic Commensalism and
996 Competition in a Two-Species Microbial Consortium. Applied and Environmental
997 Microbiology 68:2495–2502.

998 37. Veseli I, Chen YT, Schechter MS, Vanni C, Fogarty EC, Watson AR, Jabri B, Blekhman R,
999 Willis AD, Yu MK, Fernàndez-Guerra A, Füssel J, Eren AM. 2023. Microbes with higher
1000 metabolic independence are enriched in human gut microbiomes under stress. eLife 12.

1001 38. Arellano AA, Young EB, Coon KL. 2024. An inquiline mosquito modulates microbial
1002 diversity and function in an aquatic microecosystem. Molecular Ecology 33:e17314.

1003 39. Langenheder S, Lindström ES, Tranvik LJ. 2005. Weak coupling between community
1004 composition and functioning of aquatic bacteria. Limnology and Oceanography 50:957–
1005 967.

1006 40. Morris C, Kinkel L. 2002. Fifty years of phyllosphere microbiology: Significant
1007 contributions to research in related fields. Phyllosphere Microbiology 365–375.

1008 41. Grothjan JJ, Young EB. 2019. Diverse microbial communities hosted by the model
1009 carnivorous pitcher plant *Sarracenia purpurea*: analysis of both bacterial and eukaryotic
1010 composition across distinct host plant populations. PeerJ 7:e6392.

1011 42. Armitage DW. 2017. Linking the development and functioning of a carnivorous pitcher
1012 plant's microbial digestive community. 11. The ISME Journal 11:2439–2451.

1013 43. Shobade SO, Zabotina OA, Nilsen-Hamilton M. 2024. Plant root associated chitinases:
1014 structures and functions. Front Plant Sci 15.

1015 44. Dewangan BP, Gupta A, Sah RK, Das S, Kumar S, Bhattacharjee S, Pawar PA-M. 2023.
1016 Xylobiose treatment triggers a defense-related response and alters cell wall composition.
1017 Plant Mol Biol 113:383–400.

1018 45. Ng LC, Sariah M, Sariam O, Radziah O, Zainal Abidin MA. 2016. PGPM-induced defense-
1019 related enzymes in aerobic rice against rice leaf blast caused by Pyricularia oryzae. Eur J
1020 Plant Pathol 145:167–175.

1021 46. Naseem S, Parrino SM, Buenten DM, Konopka JB. 2012. Novel roles for GlcNAc in cell
1022 signaling. Commun Integr Biol 5:156–159.

1023 47. Beier S, Bertilsson S. 2013. Bacterial chitin degradation—mechanisms and
1024 ecophysiological strategies. Frontiers in Microbiology 4.

1025 48. Jiang W-X, Li P-Y, Chen X-L, Zhang Y-S, Wang J-P, Wang Y-J, Sheng Q, Sun Z-Z, Qin Q-L, Ren
1026 X-B, Wang P, Song X-Y, Chen Y, Zhang Y-Z. 2022. A pathway for chitin oxidation in marine
1027 bacteria. 1. Nat Commun 13:5899.

1028 49. Li J, Gu S, Zhao Z, Chen B, Liu Q, Sun T, Sun W, Tian C. 2019. Dissecting cellobiose
1029 metabolic pathway and its application in biorefinery through consolidated bioprocessing
1030 in Myceliophthora thermophila. Fungal Biology and Biotechnology 6:21.

1031 50. Peterson CN, Day S, Wolfe BE, Ellison AM, Kolter R, Pringle A. 2008. A keystone predator
1032 controls bacterial diversity in the pitcher-plant (Sarracenia purpurea) microecosystem.
1033 Environmental Microbiology 10:2257–2266.

1034 51. Bittleston LS, Gralka M, Leventhal GE, Mizrahi I, Cordero OX. 2020. Context-dependent
1035 dynamics lead to the assembly of functionally distinct microbial communities. Nat
1036 Commun 11:1440.

1037 52. Ueno H, Miyashita K. 2000. Inductive production of chitinolytic enzymes in soil
1038 microcosms using chitin, other carbon-sources, and chitinase-producing *Streptomyces*.
1039 Soil Science and Plant Nutrition 46:863–871.

1040 53. Brewster JD. 2003. A simple micro-growth assay for enumerating bacteria. Journal of
1041 Microbiological Methods 53:77–86.

1042 54. Sprouffske K, Wagner A. 2016. Growthcurver: an R package for obtaining interpretable
1043 metrics from microbial growth curves. BMC Bioinformatics 17:172.

1044 55. Campbell CD, Chapman SJ, Cameron CM, Davidson MS, Potts JM. 2003. A Rapid
1045 Microtiter Plate Method To Measure Carbon Dioxide Evolved from Carbon Substrate
1046 Amendments so as To Determine the Physiological Profiles of Soil Microbial Communities
1047 by Using Whole Soil. Applied and Environmental Microbiology 69:3593–3599.

1048 56. Ellison AM, Gotelli NJ. 2002. Nitrogen availability alters the expression of carnivory in the
1049 northern pitcher plant, Sarracenia purpurea. PNAS 99:4409–4412.

1050 57. Maxwell K, Johnson GN. 2000. Chlorophyll fluorescence—a practical guide. Journal of
1051 Experimental Botany 51:659–668.

1052 58. Caporaso JG, Lauber CL, Walters WA, Berg-Lyons D, Lozupone CA, Turnbaugh PJ, Fierer N,
1053 Knight R. 2011. Global patterns of 16S rRNA diversity at a depth of millions of sequences
1054 per sample. Proc Natl Acad Sci USA 108:4516–4522.

1055 59. Callahan BJ, McMurdie PJ, Rosen MJ, Han AW, Johnson AJA, Holmes SP. 2016. DADA2:
1056 High resolution sample inference from Illumina amplicon data. Nat Methods 13:581–583.

1057 60. Bolyen E, Rideout JR, Dillon MR, Bokulich NA, Abnet CC, Al-Ghalith GA, Alexander H, Alm
1058 EJ, Arumugam M, Asnicar F, Bai Y, Bisanz JE, Bittinger K, Brejnrod A, Brislawn CJ, Brown
1059 CT, Callahan BJ, Caraballo-Rodríguez AM, Chase J, Cope EK, Da Silva R, Diener C,
1060 Dorrestein PC, Douglas GM, Durall DM, Duvallet C, Edwardson CF, Ernst M, Estaki M,
1061 Fouquier J, Gauglitz JM, Gibbons SM, Gibson DL, Gonzalez A, Gorlick K, Guo J, Hillmann B,
1062 Holmes S, Holste H, Huttenhower C, Huttley GA, Janssen S, Jarmusch AK, Jiang L, Kaehler
1063 BD, Kang KB, Keefe CR, Keim P, Kelley ST, Knights D, Koester I, Kosciolek T, Kreps J,
1064 Langille MGI, Lee J, Ley R, Liu Y-X, Loftfield E, Lozupone C, Maher M, Marotz C, Martin BD,
1065 McDonald D, McIver LJ, Melnik AV, Metcalf JL, Morgan SC, Morton JT, Naimey AT, Navas-
1066 Molina JA, Nothias LF, Orchanian SB, Pearson T, Peoples SL, Petras D, Preuss ML, Pruesse
1067 E, Rasmussen LB, Rivers A, Robeson MS, Rosenthal P, Segata N, Shaffer M, Shiffer A,
1068 Sinha R, Song SJ, Spear JR, Swafford AD, Thompson LR, Torres PJ, Trinh P, Tripathi A,
1069 Turnbaugh PJ, Ul-Hasan S, van der Hooft JJJ, Vargas F, Vázquez-Baeza Y, Vogtmann E, von
1070 Hippel M, Walters W, Wan Y, Wang M, Warren J, Weber KC, Williamson CHD, Willis AD,

1071 Xu ZZ, Zaneveld JR, Zhang Y, Zhu Q, Knight R, Caporaso JG. 2019. Reproducible,
1072 interactive, scalable and extensible microbiome data science using QIIME 2. 8. Nat
1073 Biotechnol 37:852–857.

1074 61. McDonald D, Price MN, Goodrich J, Nawrocki EP, DeSantis TZ, Probst A, Andersen GL,
1075 Knight R, Hugenholtz P. 2012. An improved Greengenes taxonomy with explicit ranks for
1076 ecological and evolutionary analyses of bacteria and archaea. 3. ISME J 6:610–618.

1077 62. Katoh K. 2002. MAFFT: a novel method for rapid multiple sequence alignment based on
1078 fast Fourier transform. Nucleic Acids Research 30:3059–3066.

1079 63. Price MN, Dehal PS, Arkin AP. 2009. FastTree: Computing Large Minimum Evolution Trees
1080 with Profiles instead of a Distance Matrix. Molecular Biology and Evolution 26:1641–
1081 1650.

1082 64. McMurdie PJ, Holmes S. 2013. phyloseq: An R Package for Reproducible Interactive
1083 Analysis and Graphics of Microbiome Census Data. PLOS ONE 8:e61217.

1084 65. Bisanz, Jordan E. 2018. qiime2R: Importing QIIME2 artifacts and associated data into R
1085 sessions.

1086 66. Kembel SW, Ackerly DD, Blomberg SP, Cornwell WK, Cowan PD, Helmus MR, Morlon H,
1087 Webb CO. 2020. picante: Integrating Phylogenies and Ecology (1.8.2).

1088 67. Davis NM, Proctor DM, Holmes SP, Relman DA, Callahan BJ. 2018. Simple statistical
1089 identification and removal of contaminant sequences in marker-gene and metagenomics
1090 data. Microbiome 6:226.

1091 68. Bürkner P-C. 2018. Advanced Bayesian Multilevel Modeling with the R Package brms. The
1092 R Journal 10:395.

1093 69. Andrews S. 2010. FastQC: A Quality Control Tool for High Throughput Sequence Data
1094 [Online].

1095 70. Bolger AM, Lohse M, Usadel B. 2014. Trimmomatic: a flexible trimmer for Illumina
1096 sequence data. Bioinformatics 30:2114–2120.

1097 71. Ewels P, Magnusson M, Lundin S, Käller M. 2016. MultiQC: summarize analysis results for
1098 multiple tools and samples in a single report. Bioinformatics 32:3047–3048.

1099 72. Deng Z-L, Münch PC, Mreches R, McHardy AC. 2022. Rapid and accurate identification of
1100 ribosomal RNA sequences via deep learning. Nucleic Acids Res 50:e60.

1101 73. Li D, Liu C-M, Luo R, Sadakane K, Lam T-W. 2015. MEGAHIT: an ultra-fast single-node
1102 solution for large and complex metagenomics assembly via succinct de Bruijn graph.
1103 Bioinformatics 31:1674–1676.

1104 74. Li D, Luo R, Liu C-M, Leung C-M, Ting H-F, Sadakane K, Yamashita H, Lam T-W. 2016.
1105 MEGAHIT v1.0: A fast and scalable metagenome assembler driven by advanced
1106 methodologies and community practices. Methods 102:3–11.

1107 75. Brown CT, Irber L. 2016. sourmash: a library for MinHash sketching of DNA. Journal of
1108 Open Source Software 1:27.

1109 76. Parks DH, Chuvochina M, Rinke C, Mussig AJ, Chaumeil P-A, Hugenholtz P. 2022. GTDB:
1110 an ongoing census of bacterial and archaeal diversity through a phylogenetically
1111 consistent, rank normalized and complete genome-based taxonomy. Nucleic Acids
1112 Research 50:D785–D794.

1113 77. Alneberg J, Bjarnason BS, de Bruijn I, Schirmer M, Quick J, Ijaz UZ, Lahti L, Loman NJ,
1114 Andersson AF, Quince C. 2014. Binning metagenomic contigs by coverage and
1115 composition. Nat Methods 11:1144–1146.

1116 78. Wu Y-W, Simmons BA, Singer SW. 2016. MaxBin 2.0: an automated binning algorithm to
1117 recover genomes from multiple metagenomic datasets. Bioinformatics 32:605–607.

1118 79. Sieber CMK, Probst AJ, Sharrar A, Thomas BC, Hess M, Tringe SG, Banfield JF. 2018.
1119 Recovery of genomes from metagenomes via a dereplication, aggregation and scoring
1120 strategy. 7. Nat Microbiol 3:836–843.

1121 80. Kang DD, Li F, Kirton E, Thomas A, Egan R, An H, Wang Z. 2019. MetaBAT 2: an adaptive
1122 binning algorithm for robust and efficient genome reconstruction from metagenome
1123 assemblies. PeerJ 7:7359.

1124 81. Chklovski A, Parks DH, Woodcroft BJ, Tyson GW. 2023. CheckM2: a rapid, scalable and
1125 accurate tool for assessing microbial genome quality using machine learning. Nature
1126 Methods 20:1203–1212.

1127 82. Olm MR, Brown CT, Brooks B, Banfield JF. 2017. dRep: a tool for fast and accurate
1128 genomic comparisons that enables improved genome recovery from metagenomes
1129 through de-replication. 12. ISME J 11:2864–2868.

1130 83. Campbell JH, O'Donoghue P, Campbell AG, Schwientek P, Sczyrba A, Woyke T, Söll D,
1131 Podar M. 2013. UGA is an additional glycine codon in uncultured SR1 bacteria from the
1132 human microbiota. Proceedings of the National Academy of Sciences 110:5540–5545.

1133 84. Bowers RM, Kyrpides NC, Stepanauskas R, Harmon-Smith M, Doud D, Reddy TBK, Schulz
1134 F, Jarett J, Rivers AR, Eloe-Fadrosh EA, Tringe SG, Ivanova NN, Copeland A, Clum A,
1135 Becraft ED, Malmstrom RR, Birren B, Podar M, Bork P, Weinstock GM, Garrity GM,
1136 Dodsworth JA, Yooseph S, Sutton G, Glöckner FO, Gilbert JA, Nelson WC, Hallam SJ,
1137 Jungbluth SP, Ettema TJG, Tighe S, Konstantinidis KT, Liu W-T, Baker BJ, Rattei T, Eisen JA,
1138 Hedlund B, McMahon KD, Fierer N, Knight R, Finn R, Cochrane G, Karsch-Mizrachi I, Tyson
1139 GW, Rinke C, Lapidus A, Meyer F, Yilmaz P, Parks DH, Murat Eren A, Schriml L, Banfield JF,
1140 Hugenholtz P, Woyke T. 2017. Minimum information about a single amplified genome
1141 (MISAG) and a metagenome-assembled genome (MIMAG) of bacteria and archaea. 8.
1142 Nat Biotechnol 35:725–731.

1143 85. Li H, Durbin R. 2009. Fast and accurate short read alignment with Burrows–Wheeler
1144 transform. Bioinformatics 25:1754–1760.

1145 86. Danecek P, Bonfield JK, Liddle J, Marshall J, Ohan V, Pollard MO, Whitwham A, Keane T,
1146 McCarthy SA, Davies RM, Li H. 2021. Twelve years of SAMtools and BCFtools. GigaScience
1147 10:8.

1148 87. Nguyen L-T, Schmidt HA, von Haeseler A, Minh BQ. 2015. IQ-TREE: A Fast and Effective
1149 Stochastic Algorithm for Estimating Maximum-Likelihood Phylogenies. Mol Biol Evol
1150 32:268–274.

1151 88. Altschul SF, Gish W, Miller W, Myers EW, Lipman DJ. 1990. Basic local alignment search
1152 tool. J Mol Biol 215:403–410.

1153 89. Shen W, Le S, Li Y, Hu F. 2016. SeqKit: A Cross-Platform and Ultrafast Toolkit for FASTA/Q
1154 File Manipulation. PLoS ONE 11:e0163962.

1155 90. Rognes T, Flouri T, Nichols B, Quince C, Mahé F. 2016. VSEARCH: a versatile open source
1156 tool for metagenomics. PeerJ 4:e2584.

1157 91. Hyatt D, Chen G-L, LoCascio PF, Land ML, Larimer FW, Hauser LJ. 2010. Prodigal:
1158 prokaryotic gene recognition and translation initiation site identification. BMC
1159 Bioinformatics 11:119.

1160 92. Bray NL, Pimentel H, Melsted P, Pachter L. 2016. Near-optimal probabilistic RNA-seq
1161 quantification. 5. Nat Biotechnol 34:525–527.

1162 93. Aramaki T, Blanc-Mathieu R, Endo H, Ohkubo K, Kanehisa M, Goto S, Ogata H. 2020.
1163 KofamKOALA: KEGG Ortholog assignment based on profile HMM and adaptive score
1164 threshold. Bioinformatics 36:2251–2252.

1165 94. Law CW, Chen Y, Shi W, Smyth GK. 2014. voom: precision weights unlock linear model
1166 analysis tools for RNA-seq read counts. Genome Biology 15:R29.

1167 95. R Core Team. 2019. R: A Language and Environment for Statistical Computing. R
1168 Foundation for Statistical Computing, Vienna, Austria. https://www.R-project.org/.

1169 96. Oksanen J, Blanchet FG, Friendly M, Kindt R, Legendre P, McGlinn D, Minchin PR, O'Hara
1170 RB, Simpson GL, Solymos P, Stevens MHH, Szoecs E, Wagner H. 2019. vegan: Community
1171 Ecology Package. https://CRAN.R-project.org/package=vegan.

1172 97. Wickham H. 2020. reshape2: Flexibly Reshape Data: A Reboot of the Reshape Package
1173 (1.4.4).

1174 98. Firke S, Denney B, Haid C, Knight R, Grosser M, Zadra J. 2023. janitor: Simple Tools for
1175 Examining and Cleaning Dirty Data (2.2.0).

1176 99. Wickham H, RStudio. 2023. tidyverse: Easily Install and Load the "Tidyverse" (2.0.0).

1177 100. Kolde R. 2019. pheatmap: Pretty Heatmaps (1.0.12).

1178 101. Lozupone C, Lladser ME, Knights D, Stombaugh J, Knight R. 2011. UniFrac: an effective
1179 distance metric for microbial community comparison. 2. ISME J 5:169–172.

1180 102. Cinner JE, Huchery C, MacNeil MA, Graham NAJ, McClanahan TR, Maina J, Maire E,
1181 Kittinger JN, Hicks CC, Mora C, Allison EH, D'Agata S, Hoey A, Feary DA, Crowder L,
1182 Williams ID, Kulbicki M, Vigliola L, Wantiez L, Edgar G, Stuart-Smith RD, Sandin SA, Green
1183 AL, Hardt MJ, Beger M, Friedlander A, Campbell SJ, Holmes KE, Wilson SK, Brokovich E,
1184 Brooks AJ, Cruz-Motta JJ, Booth DJ, Chabanet P, Gough C, Tupper M, Ferse SCA, Sumaila
1185 UR, Mouillot D. 2016. Bright spots among the world's coral reefs. Nature 535:416–419.

1186 103. Kimmel K, Dee LE, Avolio ML, Ferraro PJ. 2021. Causal assumptions and causal inference
1187 in ecological experiments. Trends in Ecology & Evolution 36:1141–1152.

1188 104. McElreath R. 2016. Statistical Rethinking: A Bayesian Course with Examples in R and Stan.
1189 Chapman and Hall/CRC, New York.

1190 105. Lüdecke D. 2018. ggeffects: Tidy Data Frames of Marginal Effects from Regression
1191 Models. Journal of Open Source Software 3:772.

1192 106. Gabry J, Mahr T, Bürkner P-C, Modrák M, Barrett M, Weber F, Sroka EC, Sailynoja T,
1193 Vehtari A. 2022. bayesplot: Plotting for Bayesian Models (1.10.0).

1194 107. Kay M, Mastny T. 2023. tidybayes: Tidy Data and "Geoms" for Bayesian Models (3.0.6).

1195 108. Eager CD. 2021. standardize: Tools for Standardizing Variables for Regression in R (0.2.2).

1196 109. Gelman A, Hill J. 2006. Data Analysis Using Regression and Multilevel/Hierarchical
1197 Models. Cambridge University Press.

1198

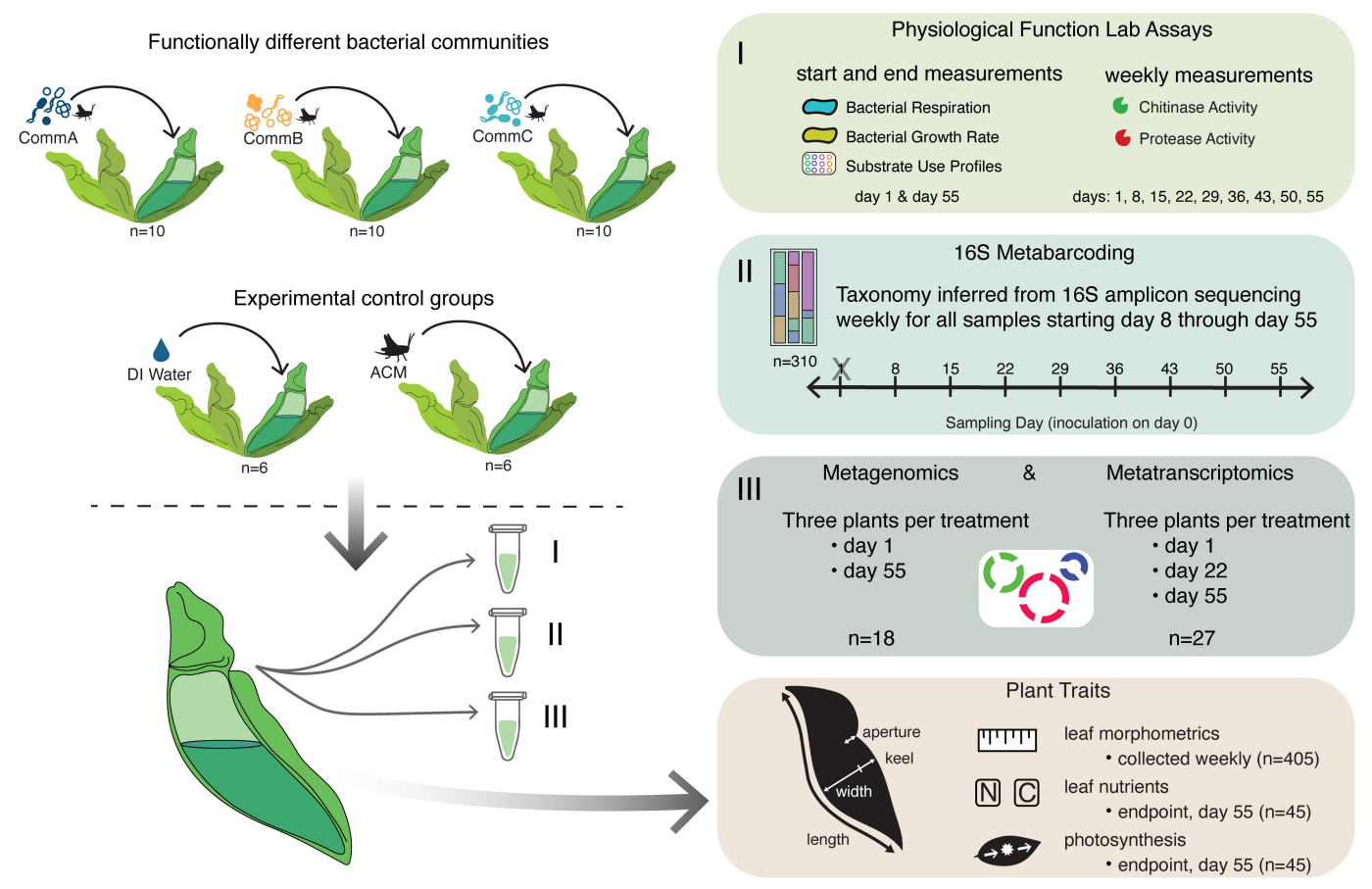
Functionally different bacterial communities
CommA
CommB
CommC
n=10
n=10
n=10
Experimental control groups
DI Water
ACM
n=6
n=6
I
II
III
Physiological Function Lab Assays
I
start and end measurements
Bacterial Respiration
Bacterial Growth Rate
Substrate Use Profiles
day 1 & day 55
weekly measurements
Chitinase Activity
Protease Activity
days: 1, 8, 15, 22, 29, 36, 43, 50, 55
16S Metabarcoding
II
Taxonomy inferred from 16S amplicon sequencing
weekly for all samples starting day 8 through day 55
n=310
8
15
22
29
36
43
50
55
Sampling Day (inoculation on day 0)
III
Metagenomics
&
Metatranscriptomics
Three plants per treatment
• day 1
• day 55
n=18
Three plants per treatment
• day 1
• day 22
• day 55
n=27
Plant Traits
aperture
keel
width
length
leaf morphometrics
• collected weekly (n=405)
N
C
leaf nutrients
• endpoint, day 55 (n=45)
photosynthesis
• endpoint, day 55 (n=45)

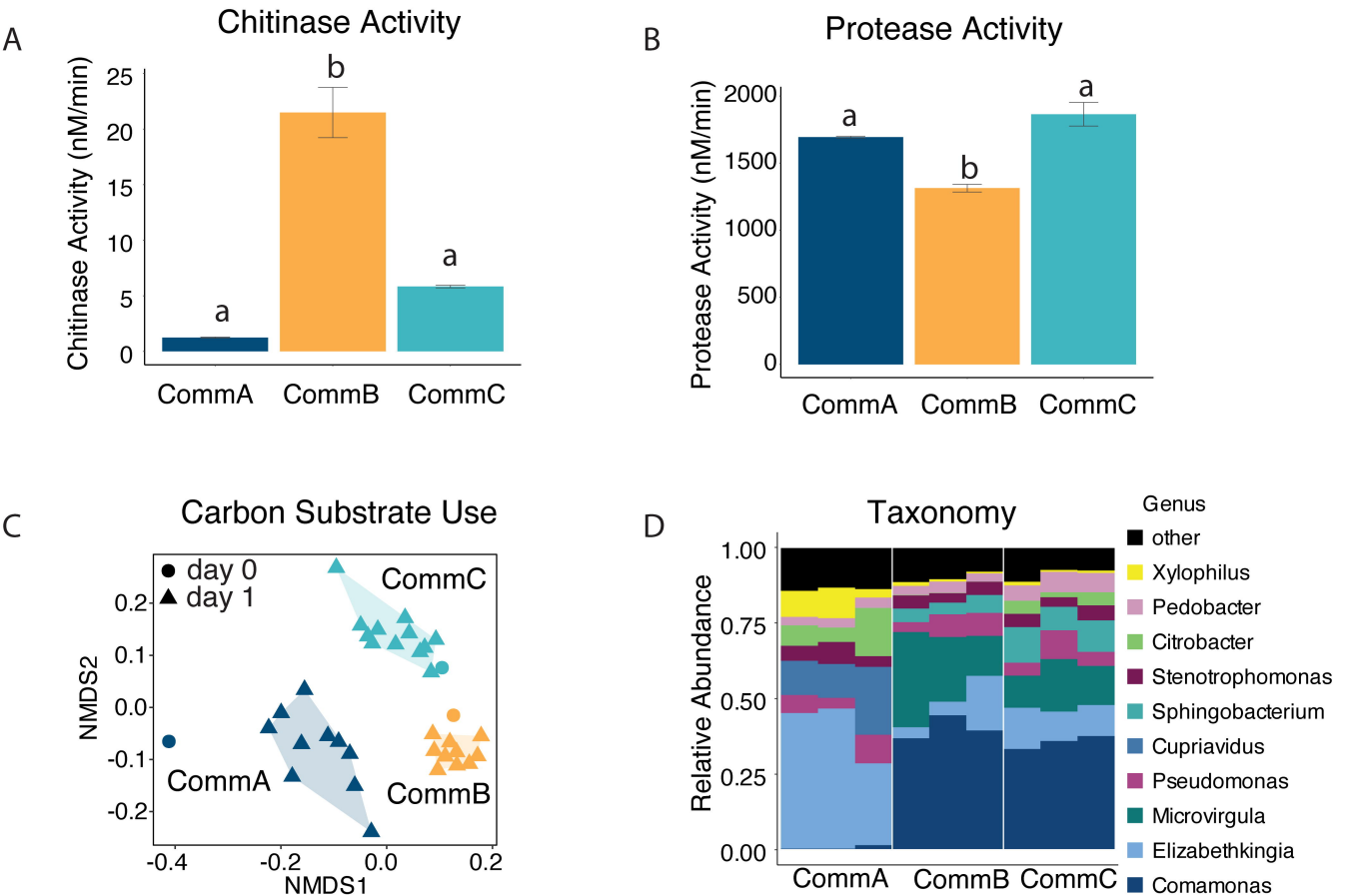
A
Chitinase Activity
Chitinase Activity (nM/min)
25
20
15
10
5
0
a
b
a
CommA
CommB
CommC
B
Protease Activity
Protease Activity (nM/min)
2000
1500
1000
500
0
a
b
a
CommA
CommB
CommC
C
Carbon Substrate Use
day 0
day 1
CommC
CommA
CommB
NMDS2
0.2
0.1
0.0
-0.1
-0.2
-0.4
-0.2
0.0
0.2
NMDS1
D
Taxonomy
Relative Abundance
1.00
0.75
0.50
0.25
0.00
CommA
CommB
CommC
Genus
other
Xylophilus
Pedobacter
Citrobacter
Stenotrophomonas
Sphingobacterium
Cupriavidus
Pseudomonas
Microvirgula
Elizabethkingia
Comamonas

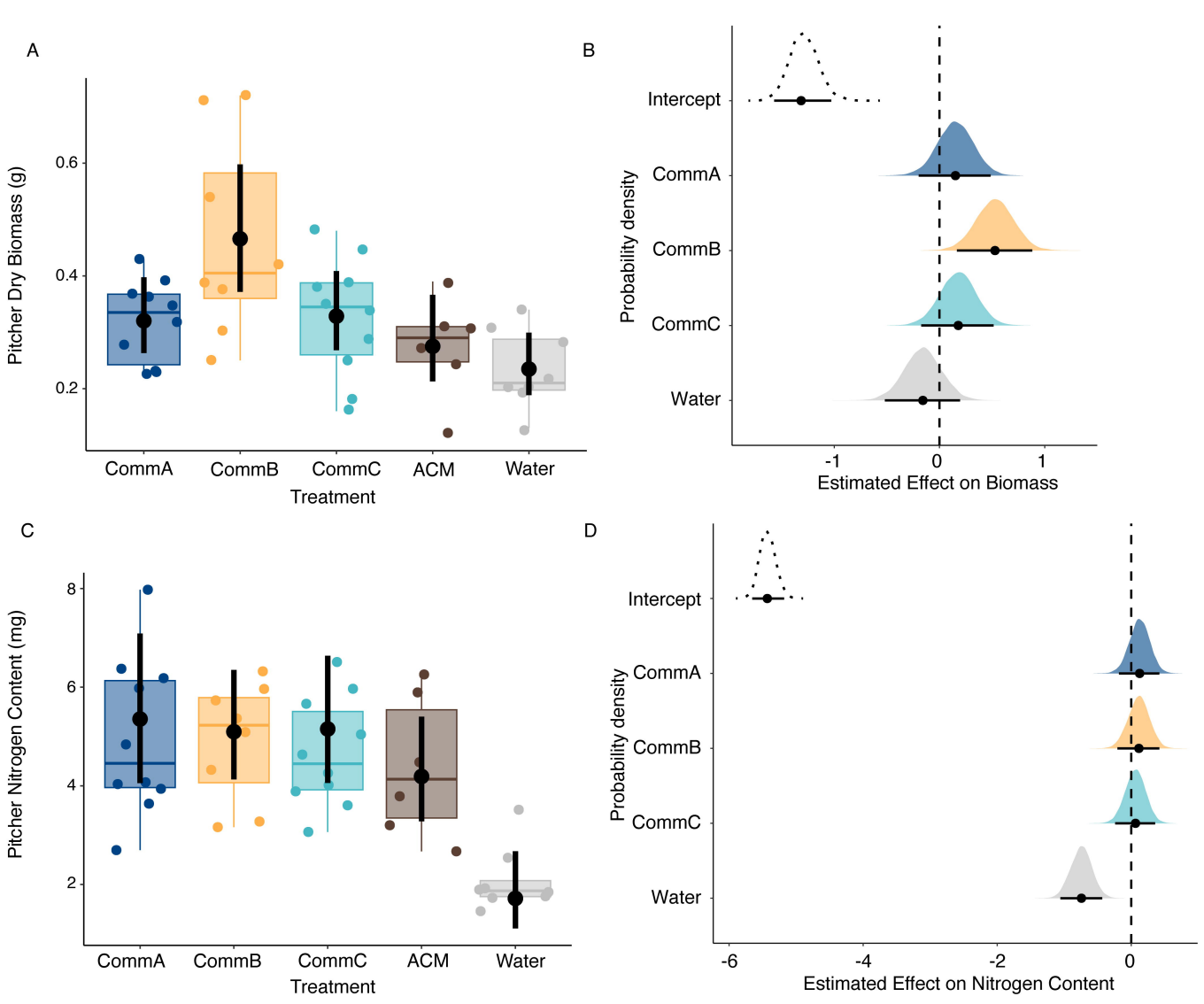
A
Pitcher Dry Biomass (g)
0.6
0.4
0.2
CommA
CommB
CommC
ACM
Water
Treatment
B
Intercept
CommA
CommB
CommC
Water
Probability density
-1
0
1
Estimated Effect on Biomass
C
Pitcher Nitrogen Content (mg)
8
6
4
2
CommA
CommB
CommC
ACM
Water
Treatment
D
Intercept
CommA
CommB
CommC
Water
Probability density
-6
-4
-2
0
Estimated Effect on Nitrogen Content

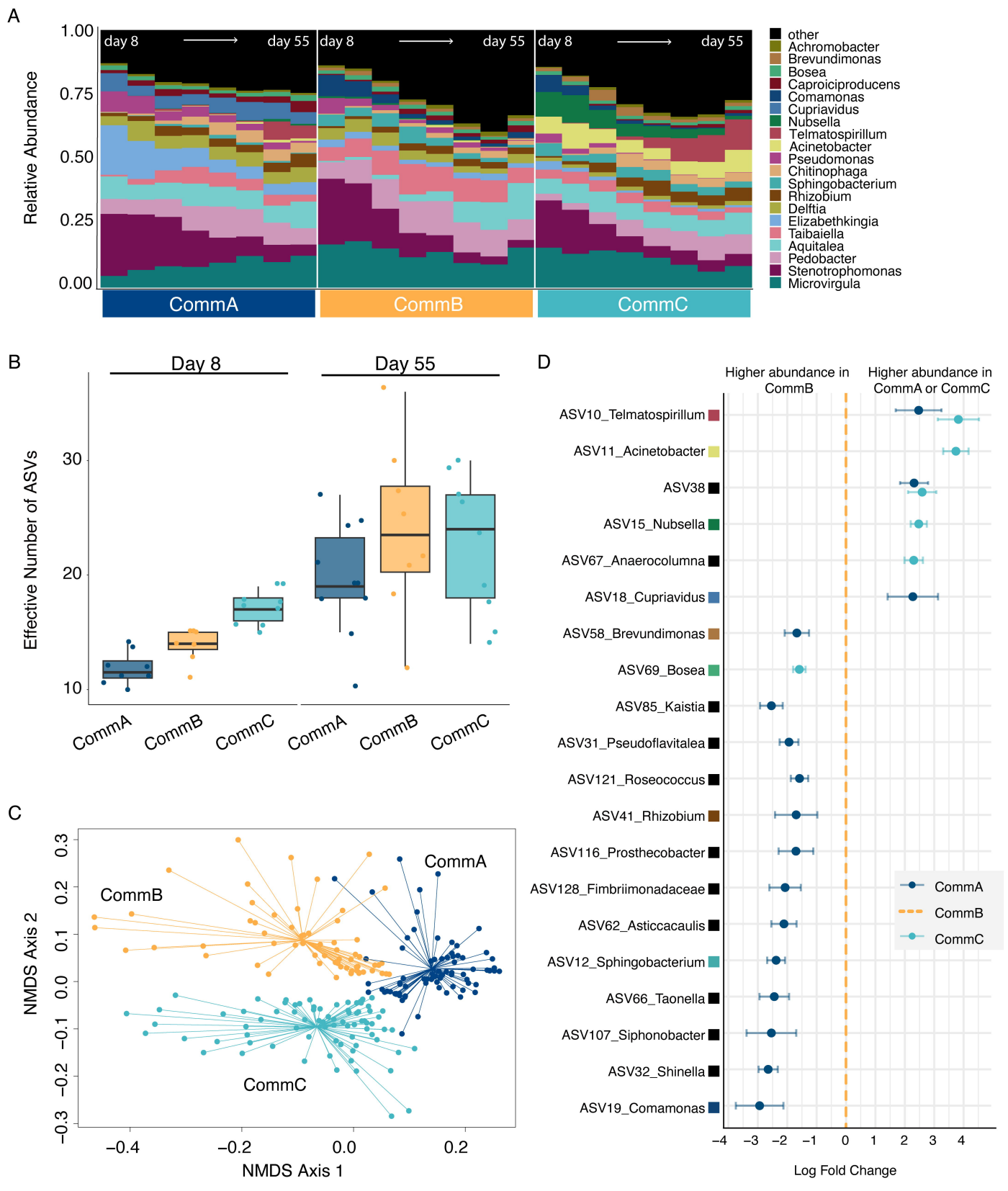
A
Relative Abundance
1.00
0.75
0.50
0.25
0.00
day 8
day 55
CommA
CommB
CommC
other
Achromobacter
Brevundimonas
Bosea
Caproiciproducens
Comamonas
Cupriavidus
Nubsella
Telmatospirillum
Acinetobacter
Pseudomonas
Chitinophaga
Sphingobacterium
Rhizobium
Delftia
Elizabethkingia
Taibaiella
Aquitalea
Pedobacter
Stenotrophomonas
Microvirgula
B
Day 8
Day 55
Effective Number of ASVs
30
20
10
CommA
CommB
CommC
C
NMDS Axis 2
NMDS Axis 1
0.3
0.2
0.1
0.0
−0.1
−0.2
−0.3
−0.4
−0.2
0.0
0.2
CommA
CommB
CommC
D
Higher abundance in CommB
Higher abundance in CommA or CommC
ASV10_Telmatospirillum
ASV11_Acinetobacter
ASV38
ASV15_Nubsella
ASV67_Anaerocolumna
ASV18_Cupriavidus
ASV58_Brevundimonas
ASV69_Bosea
ASV85_Kaistia
ASV31_Pseudoflavitalea
ASV121_Roseococcus
ASV41_Rhizobium
ASV116_Prosthecobacter
ASV128_Fimbriimonadaceae
ASV62_Asticcacaulis
ASV12_Sphingobacterium
ASV66_Taonella
ASV107_Siphonobacter
ASV32_Shinella
ASV19_Comamonas
CommA
CommB
CommC
−4
−3
−2
−1
0
1
2
3
4
Log Fold Change

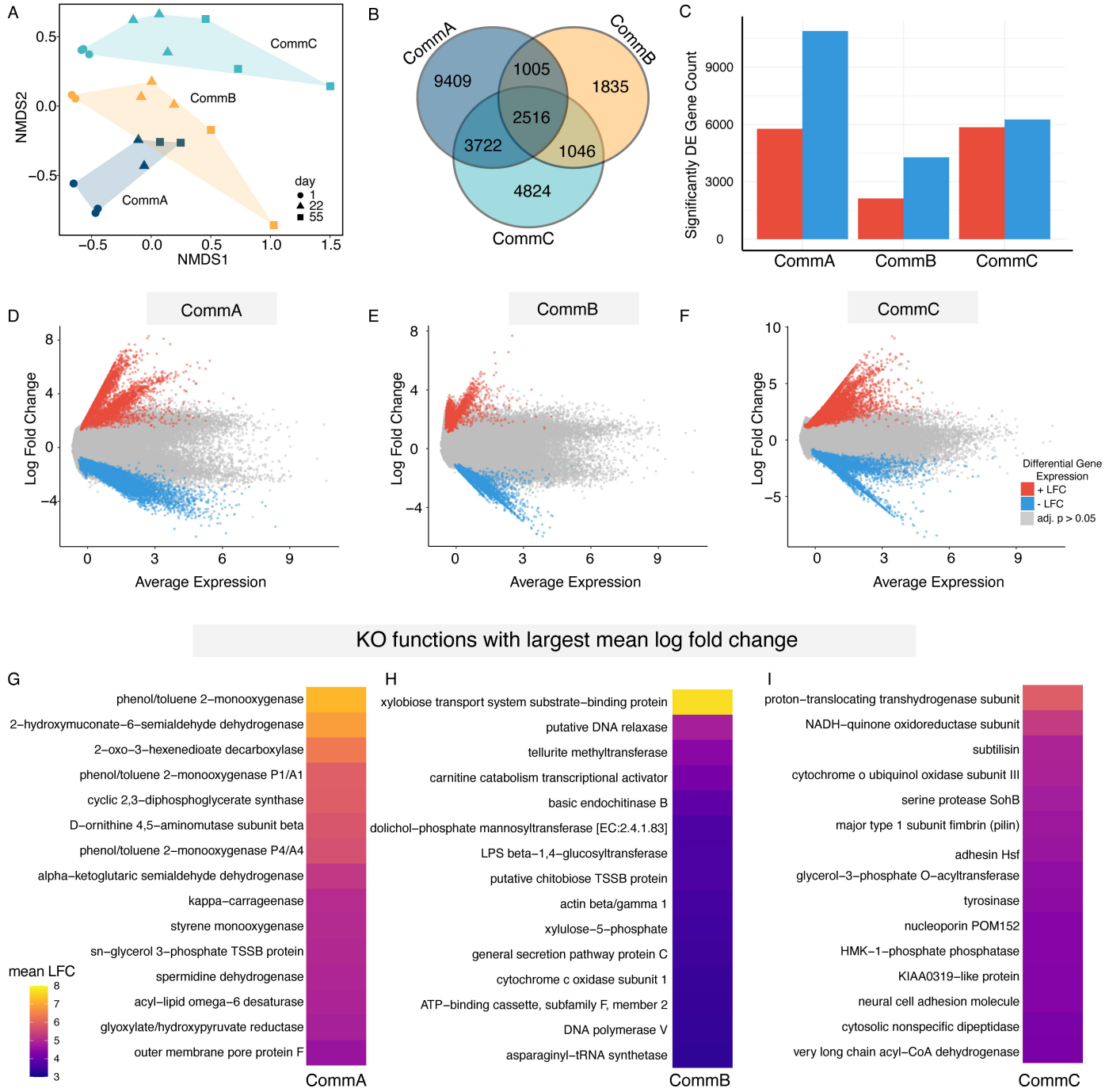
A
CommC
CommB
CommA
NMDS2
NMDS1
day
1
22
55
B
CommA
CommB
CommC
9409
1005
1835
2516
3722
1046
4824
C
Significantly DE Gene Count
CommA
CommB
CommC
D
CommA
Log Fold Change
Average Expression
E
CommB
F
CommC
Differential Gene Expression
+ LFC
- LFC
adj. p > 0.05
KO functions with largest mean log fold change
G
phenol/toluene 2−monooxygenase
2−hydroxymuconate−6−semialdehyde dehydrogenase
2−oxo−3−hexenedioate decarboxylase
phenol/toluene 2−monooxygenase P1/A1
cyclic 2,3−diphosphoglycerate synthase
D−ornithine 4,5−aminomutase subunit beta
phenol/toluene 2−monooxygenase P4/A4
alpha−ketoglutaric semialdehyde dehydrogenase
kappa−carrageenase
styrene monooxygenase
sn−glycerol 3−phosphate TSSB protein
spermidine dehydrogenase
acyl−lipid omega−6 desaturase
glyoxylate/hydroxypyruvate reductase
outer membrane pore protein F
mean LFC
H
xylobiose transport system substrate−binding protein
putative DNA relaxase
tellurite methyltransferase
carnitine catabolism transcriptional activator
basic endochitinase B
dolichol−phosphate mannosyltransferase [EC:2.4.1.83]
LPS beta−1,4−glucosyltransferase
putative chitobiose TSSB protein
actin beta/gamma 1
xylulose−5−phosphate
general secretion pathway protein C
cytochrome c oxidase subunit 1
ATP−binding cassette, subfamily F, member 2
DNA polymerase V
asparaginyl−tRNA synthetase
I
proton−translocating transhydrogenase subunit
NADH−quinone oxidoreductase subunit
subtilisin
cytochrome o ubiquinol oxidase subunit III
serine protease SohB
major type 1 subunit fimbrin (pilin)
adhesin Hsf
glycerol−3−phosphate O−acyltransferase
tyrosinase
nucleoporin POM152
HMK−1−phosphate phosphatase
KIAA0319−like protein
neural cell adhesion molecule
cytosolic nonspecific dipeptidase
very long chain acyl−CoA dehydrogenase

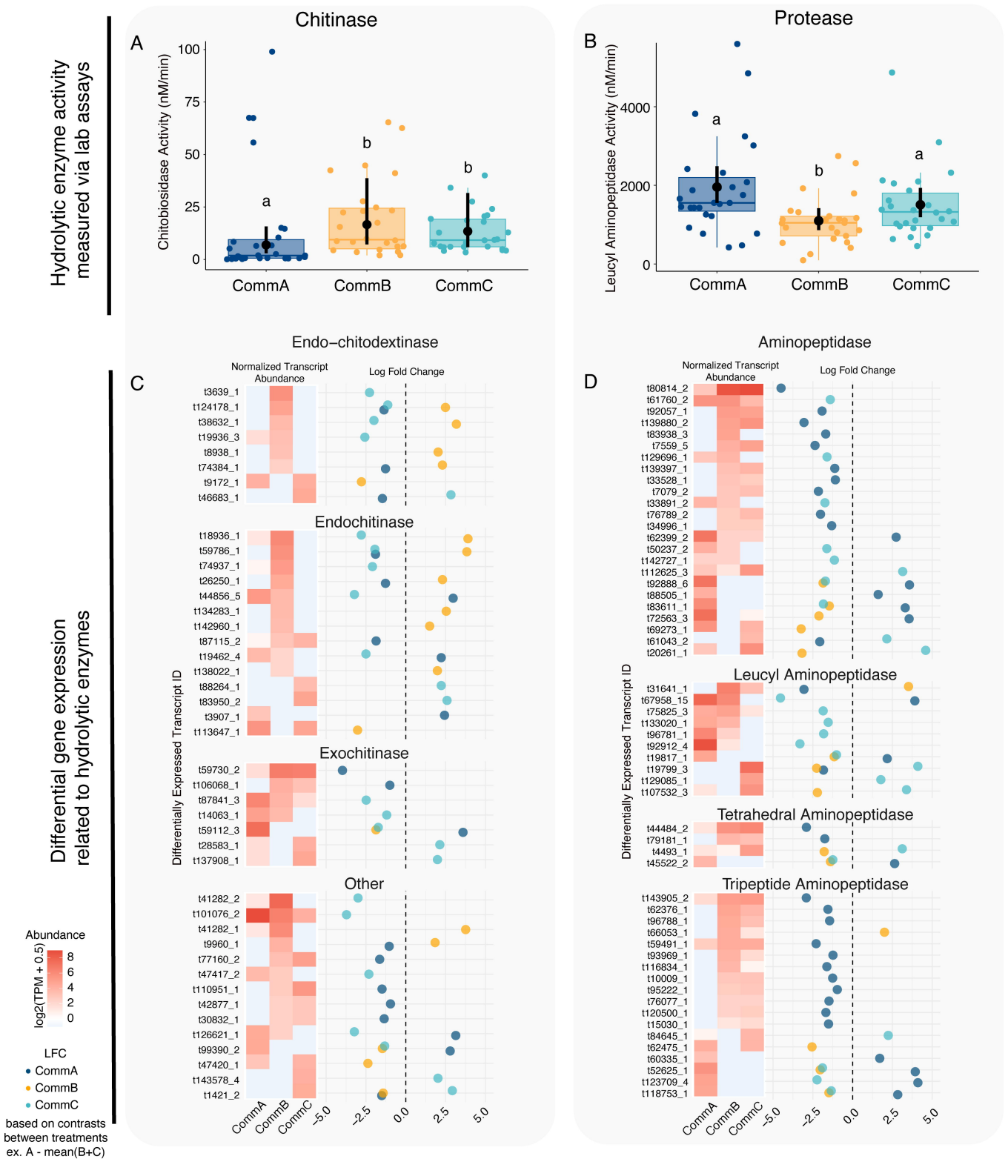
Hydrolytic enzyme activity measured via lab assays
Differential gene expression related to hydrolytic enzymes
A
Chitinase
Chitobiosidase Activity (nM/min)
100
75
50
25
0
a
b
b
CommA
CommB
CommC
B
Protease
Leucyl Aminopeptidase Activity (nM/min)
4000
2000
0
a
b
a
CommA
CommB
CommC
C
Endo−chitodextinase
Normalized Transcript Abundance
Log Fold Change
t3639_1
t124178_1
t38632_1
t19936_3
t8938_1
t74384_1
t9172_1
t46683_1
Endochitinase
t18936_1
t59786_1
t74937_1
t26250_1
t44856_5
t134283_1
t142960_1
t87115_2
t19462_4
t138022_1
t88264_1
t83950_2
t3907_1
t113647_1
Exochitinase
t59730_2
t106068_1
t87841_3
t14063_1
t59112_3
t28583_1
t137908_1
Other
t41282_2
t101076_2
t41282_1
t9960_1
t77160_2
t47417_2
t110951_1
t42877_1
t30832_1
t126621_1
t99390_2
t47420_1
t143578_4
t1421_2
Differentially Expressed Transcript ID
CommA
CommB
CommC
−5.0
−2.5
0.0
2.5
5.0
D
Aminopeptidase
Normalized Transcript Abundance
Log Fold Change
t80814_2
t61760_2
t92057_1
t139880_2
t83938_3
t7559_5
t129696_1
t139397_1
t33528_1
t7079_2
t33891_2
t76789_2
t34996_1
t62399_2
t50237_2
t142727_1
t112625_3
t92888_6
t88505_1
t83611_1
t72563_3
t69273_1
t61043_2
t20261_1
Leucyl Aminopeptidase
t31641_1
t67958_15
t75825_3
t133020_1
t96781_1
t92912_4
t19817_1
t19799_3
t129085_1
t107532_3
Tetrahedral Aminopeptidase
t44484_2
t79181_1
t4493_1
t45522_2
Tripeptide Aminopeptidase
t143905_2
t62376_1
t96788_1
t66053_1
t59491_1
t93969_1
t116834_1
t10009_1
t95222_1
t76077_1
t120500_1
t15030_1
t84645_1
t62475_1
t60335_1
t52625_1
t123709_4
t118753_1
Differentially Expressed Transcript ID
CommA
CommB
CommC
−5.0
−2.5
0.0
2.5
5.0
Abundance
log2(TPM + 0.5)
8
6
4
2
0
LFC
CommA
CommB
CommC
based on contrasts between treatments
ex. A - mean(B+C)

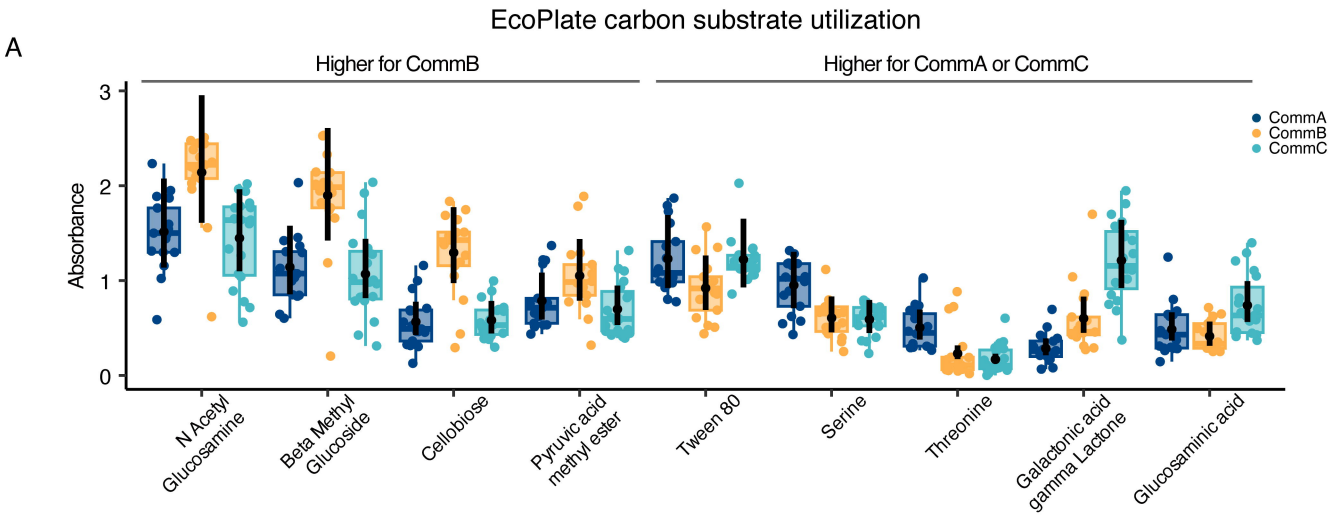
A
EcoPlate carbon substrate utilization
Higher for CommB
Higher for CommA or CommC
Absorbance
CommA
CommB
CommC
N Acetyl Glucosamine
Beta Methyl Glucoside
Cellobiose
Pyruvic acid methyl ester
Tween 80
Serine
Threonine
Galactonic acid gamma Lactone
Glucosaminic acid

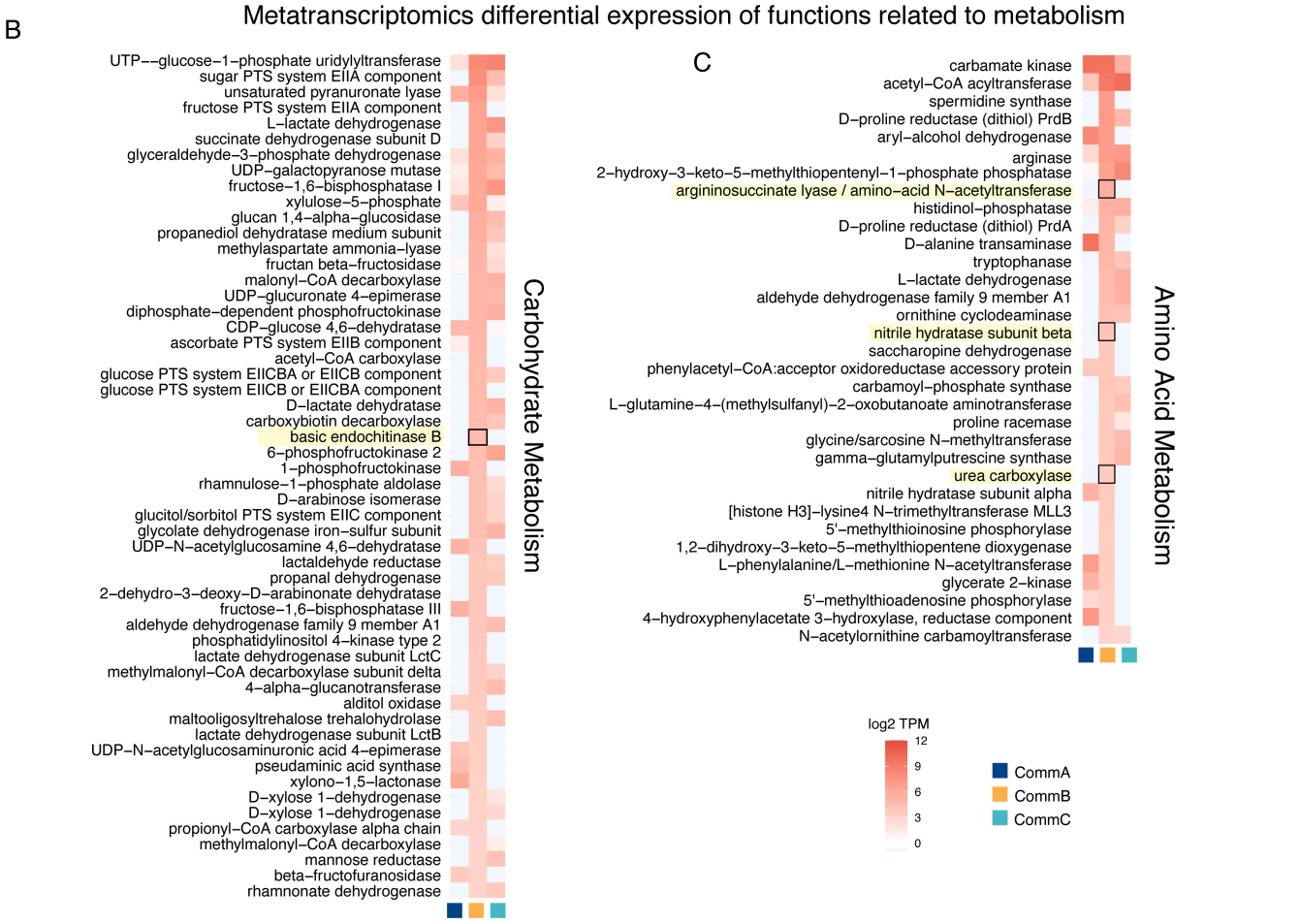
B
Metatranscriptomics differential expression of functions related to metabolism
Carbohydrate Metabolism
UTP--glucose-1-phosphate uridylyltransferase
sugar PTS system EIIA component
unsaturated pyranuronate lyase
fructose PTS system EIIA component
L-lactate dehydrogenase
succinate dehydrogenase subunit D
glyceraldehyde-3-phosphate dehydrogenase
UDP-galactopyranose mutase
fructose-1,6-bisphosphatase I
xylulose-5-phosphate
glucan 1,4-alpha-glucosidase
propanediol dehydratase medium subunit
methylaspartate ammonia-lyase
fructan beta-fructosidase
malonyl-CoA decarboxylase
UDP-glucuronate 4-epimerase
diphosphate-dependent phosphofructokinase
CDP-glucose 4,6-dehydratase
ascorbate PTS system EIIB component
acetyl-CoA carboxylase
glucose PTS system EIICBA or EIICB component
glucose PTS system EIICB or EIICBA component
D-lactate dehydratase
carboxybiotin decarboxylase
basic endochitinase B
6-phosphofructokinase 2
1-phosphofructokinase
rhamnulose-1-phosphate aldolase
D-arabinose isomerase
glucitol/sorbitol PTS system EIIC component
glycolate dehydrogenase iron-sulfur subunit
UDP-N-acetylglucosamine 4,6-dehydratase
lactaldehyde reductase
propanal dehydrogenase
2-dehydro-3-deoxy-D-arabinonate dehydratase
fructose-1,6-bisphosphatase III
aldehyde dehydrogenase family 9 member A1
phosphatidylinositol 4-kinase type 2
lactate dehydrogenase subunit LctC
methylmalonyl-CoA decarboxylase subunit delta
4-alpha-glucanotransferase
alditol oxidase
maltooligosyltrehalose trehalohydrolase
lactate dehydrogenase subunit LctB
UDP-N-acetylglucosaminuronic acid 4-epimerase
pseudaminic acid synthase
xylono-1,5-lactonase
D-xylose 1-dehydrogenase
D-xylose 1-dehydrogenase
propionyl-CoA carboxylase alpha chain
methylmalonyl-CoA decarboxylase
mannose reductase
beta-fructofuranosidase
rhamnonate dehydrogenase
C
Amino Acid Metabolism
carbamate kinase
acetyl-CoA acyltransferase
spermidine synthase
D-proline reductase (dithiol) PrdB
aryl-alcohol dehydrogenase
arginase
2-hydroxy-3-keto-5-methylthiopentenyl-1-phosphate phosphatase
argininosuccinate lyase / amino-acid N-acetyltransferase
histidinol-phosphatase
D-proline reductase (dithiol) PrdA
D-alanine transaminase
tryptophanase
L-lactate dehydrogenase
aldehyde dehydrogenase family 9 member A1
ornithine cyclodeaminase
nitrile hydratase subunit beta
saccharopine dehydrogenase
phenylacetyl-CoA:acceptor oxidoreductase accessory protein
carbamoyl-phosphate synthase
L-glutamine-4-(methylsulfanyl)-2-oxobutanoate aminotransferase
proline racemase
glycine/sarcosine N-methyltransferase
gamma-glutamylputrescine synthase
urea carboxylase
nitrile hydratase subunit alpha
[histone H3]-lysine4 N-trimethyltransferase MLL3
5'-methylthioinosine phosphorylase
1,2-dihydroxy-3-keto-5-methylthiopentene dioxygenase
L-phenylalanine/L-methionine N-acetyltransferase
glycerate 2-kinase
5'-methylthioadenosine phosphorylase
4-hydroxyphenylacetate 3-hydroxylase, reductase component
N-acetylornithine carbamoyltransferase
log2 TPM
12
9
6
3
0
CommA
CommB
CommC

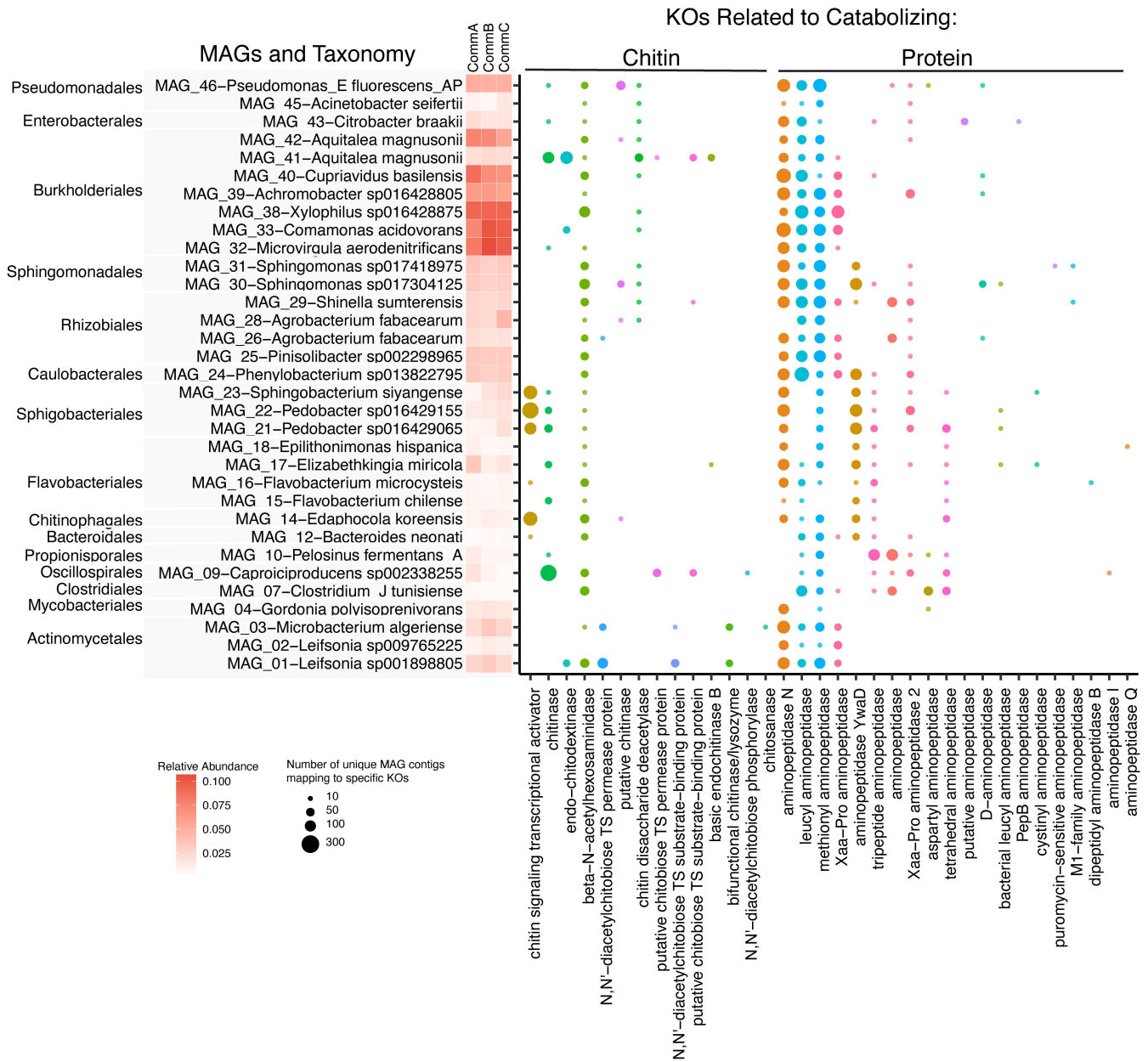
MAGs and Taxonomy
CommA
CommB
CommC
KOs Related to Catabolizing:
Chitin
Protein
Pseudomonadales
Enterobacterales
Burkholderiales
Sphingomonadales
Rhizobiales
Caulobacterales
Sphigobacteriales
Flavobacteriales
Chitinophagales
Bacteroidales
Propionisporales
Oscillospirales
Clostridiales
Mycobacteriales
Actinomycetales
MAG_46–Pseudomonas_E fluorescens_AP
MAG_45–Acinetobacter seifertii
MAG_43–Citrobacter braakii
MAG_42–Aquitalea magnusonii
MAG_41–Aquitalea magnusonii
MAG_40–Cupriavidus basilensis
MAG_39–Achromobacter sp016428805
MAG_38–Xylophilus sp016428875
MAG_33–Comamonas acidovorans
MAG_32–Microvirgula aerodenitrificans
MAG_31–Sphingomonas sp017418975
MAG_30–Sphingomonas sp017304125
MAG_29–Shinella sumterensis
MAG_28–Agrobacterium fabacearum
MAG_26–Agrobacterium fabacearum
MAG_25–Pinisolibacter sp002298965
MAG_24–Phenylobacterium sp013822795
MAG_23–Sphingobacterium siyangense
MAG_22–Pedobacter sp016429155
MAG_21–Pedobacter sp016429065
MAG_18–Epilithonimonas hispanica
MAG_17–Elizabethkingia miricola
MAG_16–Flavobacterium microcysteis
MAG_15–Flavobacterium chilense
MAG_14–Edaphocola koreensis
MAG_12–Bacteroides neonati
MAG_10–Pelosinus fermentans_A
MAG_09–Caproiciproducens sp002338255
MAG_07–Clostridium_J tunisiense
MAG_04–Gordonia polyisoprenivorans
MAG_03–Microbacterium algeriense
MAG_02–Leifsonia sp009765225
MAG_01–Leifsonia sp001898805
chitin signaling transcriptional activator
chitinase
endo–chitodextinase
beta–N–acetylhexosaminidase
N,N'–diacetylchitobiose TS permease protein
putative chitinase
chitin disaccharide deacetylase
putative chitobiose TS permease protein
N,N'–diacetylchitobiose TS substrate–binding protein
putative chitobiose TS substrate–binding protein
basic endochitinase B
bifunctional chitinase/lysozyme
N,N'–diacetylchitobiose phosphorylase
chitosanase
aminopeptidase N
leucyl aminopeptidase
methionyl aminopeptidase
Xaa–Pro aminopeptidase
aminopeptidase YwaD
tripeptide aminopeptidase
aminopeptidase
Xaa–Pro aminopeptidase 2
aspartyl aminopeptidase
tetrahedral aminopeptidase
putative aminopeptidase
D–aminopeptidase
bacterial leucyl aminopeptidase
PepB aminopeptidase
cystinyl aminopeptidase
puromycin–sensitive aminopeptidase
M1–family aminopeptidase
dipeptidyl aminopeptidase B
aminopeptidase I
aminopeptidase Q
Relative Abundance
0.100
0.075
0.050
0.025
Number of unique MAG contigs mapping to specific KOs
10
50
100
300